Heliyon 9 (2023) e15316

Contents lists available at ScienceDirect

Heliyon

journal homepage: www.cell.com/heliyon

Research article

Grain-sized moxibustion at Zusanli (ST36) promotes hepatic autophagy in rats with hyperlipidemia by regulating the ULK1 and TFEB expression through the AMPK/mTOR signaling pathway

Qian Xu [a,b], Huanxi Wu [a,b], Haibin Zhu [a,b], Chengxuan Lu [c], Jiangjia Tao [a,b], Ziqiu Zhou [a,b], Jianbin Zhang [a,b,*]

[a] Jiangsu Second Hospital of Chinese Medicine, China
[b] The Second Clinical Medical College/the Second Affiliated Hospital of Nanjing University of Chinese Medicine, China
[c] College of Acupuncture and Tuina, Nanjing University of Chinese Medicine, China

ARTICLE INFO

Keywords:
Grain-sized moxibustion
ST36
Hyperlipidemia
Hepatic autophagy
AMPK/mTOR

ABSTRACT

Objective: Grain-sized moxibustion is an effective treatment for hyperlipidemia, but how it regulates dyslipidemia and liver lipid deposits still needs to be fully understood. This study explored the molecular biological mechanism of grain-sized moxibustion to regulate hepatic autophagy in hyperlipidemic rats by affecting ULK1 and TFEB through the AMPK/mTOR signaling pathway.
Methods: Thirty male Sprague-Dawley (SD) rats were fed a high-fat diet for eight weeks to induce hyperlipidemia. Hyperlipidemic rats were divided into the HFD group, HFD + Statin group, HFD + CC + Moxi group, and grain-sized moxibustion intervention group (HFD + Moxi group). The control (Blank) group consisted of normal rats without any intervention. Grain-sized moxibustion and drug interventions were initiated eight weeks after high-fat diet induction and continued for ten weeks. Serum total cholesterol (TC), triglyceride (TG), low-density lipoprotein (LDL), and high-density lipoprotein (HDL), as well as hepatic triglyceride (TG), were measured after treatment. Hepatic steatosis and the expression of LC3I, LC3II, p62, p-AMPK, AMPK, p-mTOR, mTOR, ULK1, p-ULK1, and TFEB in the liver were analyzed.
Results: Compared with the HFD group, grain-sized moxibustion improved hyperlipidemia and hepatocyte steatosis, increased the LC3, p-AMPK, p-ULK1, and nuclear TFEB expression in the liver, but decreased the p62 and p-mTOR expression.
Conclusion: Grain-sized moxibustion at ST36 acupoints could regulate the blood lipid level of SD rats with hyperlipidemia, increase the expression level of ULK1 and TFEB by activating the AMPK/mTOR signaling pathway in liver tissues, and initiate the transcription of autophagy genes such as LC3.

1. Introduction

Hyperlipidemia refers to the disease featuring an excess blood lipid level and increased levels of total cholesterol (TC), triglyceride (TG), and low-density lipoprotein cholesterol (LDL-C) [1], which is the leading cause of the nonalcoholic fatty liver disease (NAFLD). On the one hand, the liver is the primary site of lipid synthesis; On the other hand, the comprehensive changes in blood lipid

* Corresponding author.Jiangsu Second Hospital of Chinese Medicine, China
E-mail address: zhangjianbin@njucm.edu.cn (J. Zhang).

https://doi.org/10.1016/j.heliyon.2023.e15316
Received 9 December 2022; Received in revised form 31 March 2023; Accepted 3 April 2023
Available online 14 April 2023

components are also related to liver diseases such as hepatic steatosis and NAFLD [2]. Moreover, under a high-fat diet that affects serum lipid levels and hepatocytes, fatty liver affects autophagy and degeneration [3,4]. Therefore, severe dyslipidemia may cause liver damage, inflammation, and necrosis [5].

Autophagy is a form of hepatocyte repair related to the AMP-activated protein kinase (AMPK)/mammalian target of the rapamycin (mTOR) signaling pathway. Multiple studies have shown that activation of the AMPK/mTOR signaling pathway restores autophagy regulation and alleviates NAFLD [6,7]. MTOR inhibits autophagy and is an important target in the prediction and therapy of renal cell carcinoma [8,9] and advanced urothelial cancer [10]. As shown in previous studies, liver cells play a central role in repairing a damaged liver by regulating autophagy with core autophagy proteins microtubule-associated protein light chain 3 (LC3) and Sequestosome 1 (SQSTM1, p62), kinases AMPK and mTOR, and lysosome transcription factor EB (TFEB). LC3 is involved in the formation of autophagosomes in hepatocytes [11]. As an important substrate of LC3, p62 participates in the transfer of autophagosomes to lysosomes [12]. Additionally, phosphorylated Unc-51-like kinase 1(ULk1) can regulate autophagy, and TFEB is mainly involved in the autophagic degradation or the degradation of autophagosomes in lysosomes [13,14]. These above-mentioned processes are regulated through the AMPK/mTOR signaling pathway [15]. Therefore, activation of the AMPK/mTOR signaling pathway, autophagy-related proteins LC3 and p62, and transcription factor TFEB can regulate autophagy in hepatocytes, thereby repairing liver injury caused by dyslipidemia. Regarding the autophagy and regulation mechanism, LC3I, LC3II, p62, and TFEB participate in the formation, transfer, and final degradation of autophagosomes in lysosomes, respectively, which are generally the key stages of hepatic autophagy.

Artemisia argyi leaf or Artemisia argyi velvet is used in moxibustion, the external treatment method, to burn and warm the skin surface around the acupuncture points or lesion parts after ignition, thereby promoting health and preventing and treating diseases [16,17]. Meta-analysis has shown that moxibustion is a safe and effective treatment for hyperlipidemia [18]. In the practice of traditional Chinese medicine, moxibustion stimulation at Zusanli (ST36) acupoints can effectively regulate dyslipidemia. The warm stimulation produced by moxa after ignition can directly or indirectly act on a specific skin surface region and produce certain biological effects on that region or remote parts through the transient receptor potential vanilloid (TRPV) pathway and energy metabolism pathway. Studies have demonstrated that moxibustion can affect liver lipid accumulation [19] and regulate the autophagy of various cells, including macrophages [20], cells in the spinal cord [21], the gastrointestinal tract [22], and myocardial cells [23].

However, the regulation of moxibustion on liver autophagy and its potential pathway mechanism in the case of hyperlipidemia have not been confirmed. Therefore, this study aims to explore the effect of moxibustion on liver autophagy in hyperlipidemic rats and the possible AMPK/mTOR pathway mechanism through animal experiments.

2. Materials and methods

2.1. Experimental animals

In this experiment, 30 pathogen-free Sprague Dawley (SD) rats, male, eight weeks old, and 180–220 g, were selected. Those SD rats were purchased from Shanghai Sciple-Bikai Experimental Animal Co., Ltd. [SCXK (Shanghai) 2013-0016]. The Animal Ethics Committee of Nanjing University of Chinese Medicine (ethical approval number: 201811A031) approved this study. All procedures were conducted according to the guidelines of the National Institutes of Health Animal Care and Use Committee.

2.2. Main reagents

Main reagents used in this experiment are as follows: the LDL ELISA kit (ZC-01653, Liangwei Bio); the HDL ELISA kit (ZC-01662, Liangwei Bio); the TG ELISA kit (ZC-01651, Liangwei Bio); the TC ELISA kit (ZC-02355, Liangwei Bio); immobilization solution (Servicebio, G1101); oil red dye solution (Servicebio, G1016); hematoxylin dye liquor (Servicebio, G1004); differentiation solution (Servicebio, G1005-3); blue liquid (Servicebio, G10054); glycerol gelatin capsule (Servicebio,G1402); absolute ethanol (Shanghai Jiuyi Chemical Reagent Co., Ltd., 46-17-5); xylene (Shanghai Jiuyi Chemical Reagent Co., Ltd., 1330-20-7); Su Mu (Wuhan Google Biotechnology Co., Ltd., G1004); DAB (Biyuntian Biotechnology Co., Ltd., KGP1045-100); 30% H_2O_2 (Nanjing Chemical Reagent Co., Ltd., 7722-84-1); neutral gum (Sinopharm Chemical Reagent Co., Ltd., 10004160); PVDF membranes (Millipore Company, IPVH00010); the molecular weight standard of color pre-dyed protein (Fermentas Company, 26616); Tris-Hcl/SDS (1.5 mM, pH 8.8) (Shanghai Shenggong Bioengineering Co., Ltd., SD6021); Tris-Hcl/SDS (0.5 mM, pH 6.8) (Nanjing bairui Biotechnology Co., Ltd., NJBK-022); 30% Acrylamide/Bis Solution (29:1) (Bio-RAD Company, 161-0156); SDS (Bio-Rad Company, 161-0302); AP (Bio-Rad Company, 161-0700); Tris (Bio-Rad Company, 161-0719); glycine (Bio-Rad Company, 161-0718); TEMED (Sigma Company, T8090); the ECL (enhanced chemiluminescence) Plus luminescence kit; SDS-PAGE protein loading buffer (5×); Western and IP cell lysate PMSF and BCA protein concentration determination kit (Biyuntian Company); Tween 20 (Sinopharm Chemical Reagent Co., Ltd.); NaCl (Rambo); skimmed milk powder (Yili); methanol (Chengdu Kelong Chemical Reagent Factory); goat anti-rabbit IgG-HRP (best biology, BK0027).

2.3. Preparation of moxa cones for moxibustion

The moxa cones used in the laboratory were handmade by research group members with moxa velvet as the raw material. We purchased the moxa velvet from Nanyang Boshi Trading Co., Ltd. The brand of moxa velvet we obtained is Qi Ji (registered trademark No. 21424377). The purity of moxa velvet was 80:1. According to the unified standards of moxa cones for moxibustion, moxa cones

should be weighed 0.1 g and be olive-shaped with a 4 mm long axis and a 2 mm short axis. Make the two ends slightly pointed and the middle part slightly thick. During preparation, moxa cones should be made slightly tight. Before being burned around the skin surface of rats, they should be twisted and pressed again with fingers.

2.4. Experimental drugs and preparation

(1) We used 0.5% DMSO as a solvent for atorvastatin and Compound C injection. We mixed 5 ml of DMSO standard with 995 ml of Saline to prepare the injection. (2) Atorvastatin calcium injection: Atorvastatin calcium was used for intragastric administration at 10 mg/kg each time [24]. We calculated that we needed 469.6 mg of atorvastatin standard (dry powder, 99.9%). Then, we dissolved the atorvastatin in 0.5% DMSO with 500 g of AVT in a 2 ml injection. (3) Dorsomorphin (Compound C, CC) injection: the AMPK inhibitor

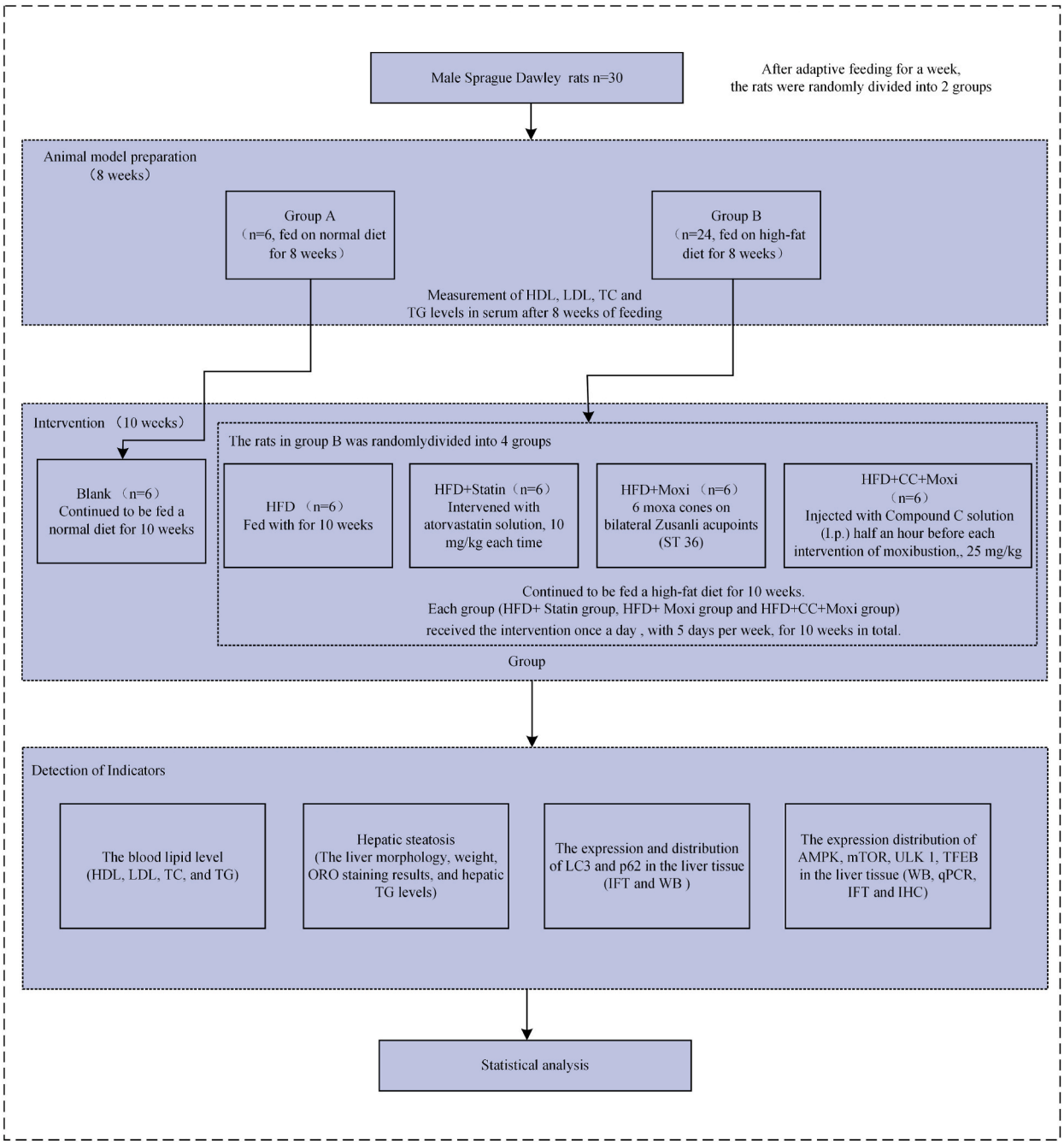

Fig. 1. The flow chart of research.

was used for intraperitoneal injection at a dose of 25 mg/kg each time [25]. Using the standard weight of each SD rat (500 g) for calculation, the CC dissolved in 0.5% DMSO should be 0.5 kg × 25 mg/kg = 12.5 mg.

2.5. Animal model preparation

According to a previous study, SD rats were fed with a high-fat diet (HFD, 41.5% lipid, 40.2% carbohydrate, and 18.3% protein, customized by Keao Xieli Feed Co., Ltd. (Beijing, China)) to induce a hyperlipidemia model [26]. Before modeling, SD rats were given adaptive feeding in the feeding room for one week, during which all SD rats were fed a normal diet (12.3% lipids, 63.3% carbohydrates, and 24.4% proteins, purchased from Keao Xieli Feed Co., Ltd.). One week later, rats in group A (6 rats) continued to be fed a normal diet, while those in group B (24 rats) began to be fed a high-fat diet with adequate water for eight weeks [27]. Euthanasia was performed at the end of the experiment (intraperitoneal injection of 25% urethane, 10 ml/kg) to minimize the suffering of animals.

2.6. Animal grouping

After the successful induction of hyperlipidemia, Group A was named Blank Group, and Group B was divided into the HFD group, HFD + Statin group, HFD + Moxi group, and HFD + CC + Moxi group according to the random number method, with six rats in each group.

2.7. Research design

After feeding rats with a high-fat diet for eight weeks, HDL, LDL, TC, and TG were tested by enzyme-linked immunosorbent assay (ELISA) to evaluate whether hyperlipidemia was successfully induced in rats. After developing hyperlipidemia, rats in the HFD group were fed a high-fat diet, while rats in the HFD + Statin group were fed a high-fat diet and intervened by intragastric administration of atorvastatin and rats in the HFD + Moxi group were fed with a high-fat diet and stimulation of ST36 acupoints by grain-sized moxibustion. Rats in the HFD + CC + Moxi group were fed a high-fat diet and injected with the Compound C inhibitor intraperitoneally before each intervention by grain-sized moxibustion.

Intragastric administration of atorvastatin, grain-sized moxibustion, and intraperitoneal injection of inhibitors was conducted after establishing hyperlipidemia (9th week). The rats in the HFD + Statin group were intervened with atorvastatin solution, with a dose of 10 mg/kg each time. The rats in the HFD + Moxi group were intervened with grain-sized moxibustion at bilateral ST 36 acupoints. According to the amount of moxa, each acupoint was stimulated with three moxa cones to avoid causing sores. The rats in the HFD + CC + Moxi group were intraperitoneally (I.p.) injected with dorsomorphin (Compound C) solution (AMPK inhibitor) at a dose of 25 mg/kg half an hour before each intervention of moxibustion. Each group (HFD + Statin group, HFD + Moxi group, and HFD + CC + Moxi group) received the intervention once a day, with two days off every five days. The entire intervention period lasted ten weeks. The frequency and duration of intragastric administration of drugs and Compound C remain the same as those of grain-sized moxibustion. See 2.8 “Intervention Methods” for more details.

At the end of the intervention period, the LDL, TC, TG, and HDL of rats in each group were tested by ELISA. The steatosis of liver cells was evaluated with Oil red O (ORO) fat staining, and the TFEB expression in liver tissues of rats in each group was tested by immunohistochemistry (IHC). The immunofluorescence technique (IFT) was used to test LC3, p62, and TFEB expression in liver tissues, and Western blotting (WB) was used to test LC3I, LC3II, p62, AMPK, mTOR, and TFEB expression. In addition, mRNA expression

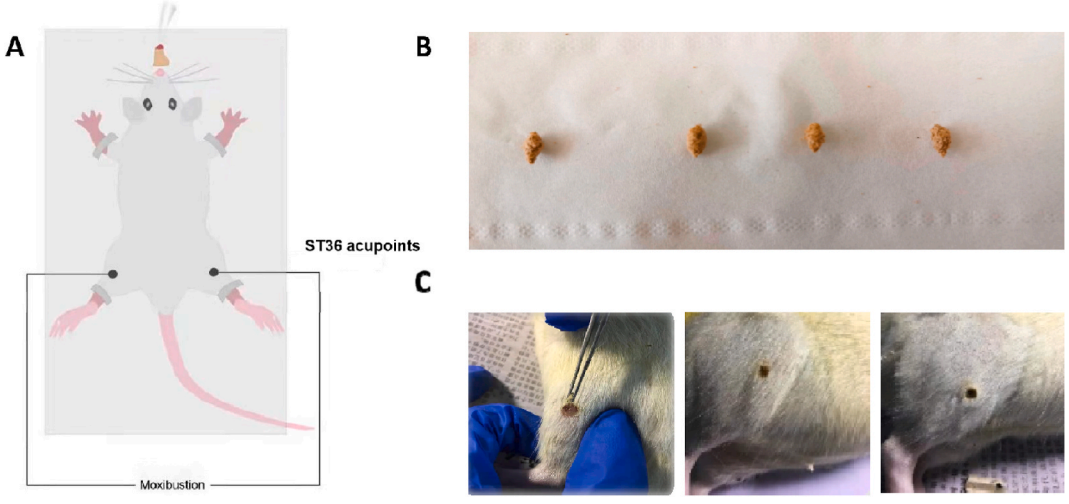

Fig. 2. Diagram of moxibustion in rats. (A) Schematic diagram of moxibustion on the ST36 acupoints in rats. (B) Grain-sized moxa cones for moxibustion intervention. (C) Grain-sized moxa cones applied to the ST36 acupoint and the ST36 acupoint after moxibustion intervention.

levels of AMPK, mTOR, and TFEB in the liver samples of rats in each group were measured through quantitative real-time PCR (qPCR). For a detailed description of each method, see 2.9 "Testing Methods." (Fig. 1).

2.8. Moxibustion intervention methods

Moxibustion intervention in ST36. One day before the first intervention of moxibustion, SD rats were anesthetized with an isoflurane gas anesthesia machine. The fur below the knee joints and above the ankle joints of rats under general anesthesia was shaved with an electric shaver to make the skin around bilateral ST36 acupoints fully exposed [28]. After SD rats were fully anesthetized with the isoflurane gas anesthesia machine, they were placed on the bench in the prone position (Fig. 2(A)). Then, a grain-sized moxa cone was put on the marked acupoint ST36 of the rat skin, ignited with string incense to burn sufficiently, and then automatically extinguished (Fig. 2(C)). The grain-sized moxa cone was wrapped with moxa floss, which is white, soft, cotton-like fibers prepared from moxa leaves (Fig. 2(B)). After the moxa cone was extinguished, the remnant ash was removed with ophthalmic forceps. During each moxibustion, three grain-sized moxa cones were burned at every acupoint. The HFD + Moxi group and HFD + CC + Moxi group received moxibustion once a day, five days per week, for ten weeks in total. After the experiment, the rats were sacrificed by intraperitoneal injection of an overdose of urethane.

2.9. Measurement of serum lipid parameters

After feeding rats with a high-fat diet for eight weeks, blood was collected from their orbits. Rats were anesthetized with isoflurane, and the retro-orbital vein was congested by compressing both sides of the neck. The capillary was rotated 45° from the medial canthus to puncture and adjusted for smooth bleeding. After blood collection, the pressure on the neck was removed, the capillary was pulled out, and the bleeding was stopped by pressing. Serum HDL, LDL, TC, and TG levels of rats in the Blank group and HFD group were tested by ELISA kit, respectively, to determine whether the hyperlipidemia model was obtained.

After the intervention, blood was collected from the abdominal aortas of rats, and levels of serum HDL, LDL, TC, and TG were tested by ELISA kit within 12 h. After anesthesia, rats were placed supine on a flat plate with their limbs fixed slightly, and the abdomen was wiped with a 5% iodine tincture. After finding the abdominal aorta, a section of the abdominal aorta of about 1.5 cm in length was separated with two vascular clips using small forceps to peel off the fascial tissue next to the open aorta. The arterial wall was lifted with small forceps at the distal end, and a blood collection tube was used for abdominal aortic puncture. When a blood return was observed, the other end was inserted into the vacuum tube, the proximal vascular clip was opened, and blood was injected.

2.10. Oil red O fat staining

Tissue samples were fixed in fixative for 15 min and covered with an OCT embedding medium. The tissues were then cut into slices and stained with oil red dye solution and hematoxylin. Each sample was examined microscopically (Olympus biologic microscope, Type BX53, 100×, 400×).

2.11. Colorimetric method

Hepatic triglyceride levels were measured using a colorimetric kit (Nanjing Jiancheng Bioengineering Institute, Nanjing, China). We performed mechanical homogenization in 10×volume of anhydrous ethanol under ice bath conditions. We removed the organic and aqueous phases and subjected the samples to centrifugation at 2500 rpm for 10 min using an Eppendorf Centrifuge (Type 5424/5424R). We removed a small aliquot (10–30 μl) and determined the triglyceride concentrations.

2.12. Immunohistochemistry

Fresh tissues were fixed in 4% paraformaldehyde for more than 24 h, and the trimmed tissues and corresponding labels were placed in a dehydration box for dehydration. The melted wax was put into the embedding frame. Before wax solidification, the tissue was taken out of the dehydration box, put into an embedding frame with a corresponding label according to the requirements of the embedding surface, and cooled at a −20 °C freezer. After solidification, the wax block was removed from the embedding frame and trimmed. Then, 4 μm sections were put in a 60 °C oven. After being dried in water, the wax was taken out and stored at room temperature for later use. The antigens were repeatedly washed and repaired with xylene, ethanol, distilled water, and phosphate buffer saline (PBS), then put into a 3% H_2O_2 solution and incubated at room temperature for 10 min to block endogenous peroxidase. The bovine serum albumin (BSA) solution was removed, and primary and secondary antibodies were added to each section. Then, 50–100 μl of freshly prepared 3,3′-diaminobenzidine (DAB) solution was added after incubation, and the color development was controlled under the microscope. The antigens were rinsed with distilled water, stained with hematoxylin for 25 s, rinsed with running water for 3–5 min, and returned to blue. After dehydration, the slides were sealed with neutral gum, dried in a fume hood, and placed under a microscope for observation and image acquisition, and analysis. Image evaluation was done by two independent observers.

2.13. Immunofluorescence

According to the method described in 2.9.3, the tissues were dehydrated, embedded, sliced, and washed with xylene, ethanol, and

PBS. The primary and secondary antibodies were added to them. The slice nuclei were stained by 4′,6-diamidino-2-phenylindole (DAPI).

2.14. Western blot

The liver tissue was transferred to a clean 1.5 ml centrifuge tube, 500 μl of PBS buffer was added, and a homogenizer was used to homogenize the tissue on an icebox (10,000 rpm, 4 °C centrifugation for 10 min). Then, the supernatant was discarded, 200 μl of Immunol precipitation (IP) lysis buffer (1 mM of phenylmethanesulfonyl fluoride (PMSF) containing resuspended cells) was added, and the lysate was transferred to a centrifuge tube with a pipette and lyse at 4 °C for 30 min. After tissue lysis, the lysate was centrifuged (4 °C, 12,000 rpm, 10 min). The supernatant was transferred to a centrifuge tube and stored at −80 °C. Then, 0.5 mg/ml of standard bovine serum albumin at the corresponding concentration was added to the standard wells. Standard dilution was added to achieve 20 μl per well. After the sample was diluted to a specific concentration with standard diluent, 20 μl was pipetted to a 96-well plate. An appropriate amount of bicinchoninic acid (BCA) working solution was prepared according to the ratio of 50 vol of BCA reagent A to 1 volume of BCA reagent B (50:1), added 200 μl to each well after mixing and placed at 37 °C for 30 min. The absorbance value was measured at 562 nm, the protein concentration of the sample was calculated according to the standard curve, and then polyacrylamide gel electrophoresis was performed. After the glass plate was cleaned and fixed on the support, 10% separating glue was poured between the glass plates, and the surface was sealed with deionized water and polymerized at room temperature. When the interface between the water seal layer and the separating glue layer was clear, the ionized water was discarded by blot-drying with filter paper, 4% stacking glue was poured in, and a comb was inserted. The comb was removed after the glue solidified. Then, a 5× loading buffer was added and mixed well. After 10 min in the metal bath, the sample was quickly put in the ice bath to cool (loading amount of 26.6 μg per lane). Electrophoresis buffer was added to the electrophoresis tank, then the power supply was turned on, and the stacking gel layer was run with 80 V constant voltage electrophoresis until the bromophenol blue ran for about 30 min. The electrophoresis voltage of the separating gel was 120 V. When the bromophenol blue migrated to the lower edge of the separating gel, the power was turned off, and the electrophoresis was stopped. Next, 1 L of transfer buffer was pre-configured and cooled to 4 °C. The polyvinylidene difluoride (PVDF) membrane was first soaked in methanol for about 30 s, then soaked in transfer buffer for 10 min, and put into electrotransfer buffer together with filter paper and gel. The sponge, filter paper, gel, PVDF membrane, filter paper, and sponge were placed in order according to the sandwich method, and all air bubbles were carefully removed. The PVDF membrane was placed on the anode side and the gel on the cathode side, inserted into the electrophoresis tank, and poured into the transfer buffer with 200 mA constant current transfer, according to the molecular weight of the transferred protein, about 1 min/kd. The PVDF membrane was immersed in a blocking solution containing 5% skimmed milk powder, placed on a shaker to shake slowly, and then sealed at room temperature for 2 h. Next, the blocked PVDF membrane was removed, and the primary antibody was added and incubated at 4 °C overnight. The PVDF membrane was immersed in 1× TBST (tris buffered saline with tween 20) buffer and washed three times on a shaker for 8 min each time. The secondary antibody was added and incubated on a shaker at room temperature for 1.5 h. The PVDF membrane was put on the plastic wrap. After mixing, an appropriate amount of solution A and solution B in the medium volume of the ECL kit was added to the surface of the membrane. The membrane was transferred to a gel imaging analyzer and exposed and developed in a chemical photosensitive mode. Image evaluation was done by two independent observers. The antibodies used include LC3 (1:2000, L7543, Sigma, USA), p62 (1:2000, PM045, MBL, Japan), glyceraldehyde-3-phosphate dehydrogenase (GAPDH) (1:1000, ta-08, ZSGB-BIO, China), p-AMPK, AMPK, p-mTOR, mTOR (1:1000, 2535S, 2532L, 5536S, 2972S, Cell Signaling Technology, USA), p-ULK1 (1:1000, 132289, NovoPro, China), ULK1 (1:1000, WL03067, Wanleibio, China), TFEB (1:1000, 13372-1-ap, proteintech, China), and proliferating cell nuclear antigen (PCNA) (1:10000, 60097-1-lg, proteintech, China).

2.15. Real-time quantitative reverse transcription PCR

First, 300 μl of lysis solution lactated ringer's solution (RL) was added per 10–20 mg of the tissue, which was ground thoroughly with a pestle; then 590 μl of Rnase-Free ddH_2O and 10 μl of proteinase K were added to the homogenate and treated at 56 °C for 10–20 min after mixing. The supernatant was removed by centrifugation at 12,000 rpm (~13,400×*g*) for 2–5 min, and 0.5 times the volume of the supernatant with absolute ethanol was added and mixed well. The solution and the precipitate were transferred to the adsorption column CR3 for 30–60 s of centrifugation at 12,000 rpm (~13,400×*g*), and the waste liquid in the collection tube was discarded. Then, 350 μl of deproteinized solution RW1 was added to the adsorption column CR3 for 30–60 s of centrifugation at 12,000 rpm (~13,400×*g*), and the waste liquid was discarded after completion. Next, 10 μl of Dnase I stock solution was put into a new Rnase-Free centrifuge tube; 70 μl of RDD solution was added; 80 μl of Dnase I working solution was added to the center of the adsorption column CR3 and placed at room temperature for 15 min. Additionally, 350 μl of deproteinized protein was added to the adsorption column CR3 Liquid RW1, and the waste liquid was discarded after the centrifugation at 12,000 rpm (~13,400×*g*) for 30–60 s. Then, 500 μl of rinse solution RW was added to the adsorption column CR3 and placed at room temperature for 2 min. The waste liquid was discarded after centrifugation at 12,000 rpm (~13,40×*g*) for 30–60 s, and the adsorption column CR3 was put back into the collection tube. Centrifugation at 12,000 rpm (~13,400×*g*) for 2 min was conducted to discard the waste. The adsorption column CR3 was left at room temperature for a few minutes to completely dry the residual rinse solution in the adsorption material. The adsorption column CR3 was transferred to a new Rnase-Free centrifuge tube. Then, 30–100 μl of Rnase-Free dd H_2O was added to the middle of the adsorption membrane, placed at room temperature for 2 min, and centrifuged at 12,000 rpm (~13,400×*g*) for 2 min to obtain RNA solution. Taking the ratio of OD260/OD280 as an indicator to measure the degree of protein contamination, a certain amount of RNA extract was taken, Rnase-Free dd H2O was used to dilute n-fold and zero the spectrometer, and the diluted OD260 and OD280 were taken for

determination. The RNA concentration was calculated according to the following formula: Final concentration (ng/μl) = (OD260) × (dilution factor n) × 40. In addition, RT reaction solution was prepared on ice, reverse transcription reaction was performed, and cDNA was stored at −20 °C. All reactions were carried out in triplicate in 20 ml of solution. The relative expression level was normalized to the GAPDH level. Specificity was verified by melting curve analysis and agarose gel electrophoresis. The primer sequences are as follows:

Gene	Forward sequence	Reverse sequence
GAPDH	TCGTGGAGTCTACTGGCGTCTT	CATTGCTGACAATCTTGAGGGAG
AMPK	TGGAGAAAGAtgGCGACGGC	ACTCGTGCTTGCCCACCTTC
mTOR	CGTCATTCCTCTGTCCACCA	CTCAAACACCTCCACCTTCTG
ULK1	TGGAGGTGGCCGTCAAATG	CGCATAGTGTGCAGGTAGTC
TFEB	CGGCTTCCCTGGTAGGTGTC	TCATTGAtgTTGAACCTGCGTC

2.16. Statistical analysis

The experimental data were analyzed using SPSS 24.0 software, and the results are expressed as the mean ± standard deviation (mean ± SD). Independent sample t-tests were used to compare data between groups. One-way ANOVA (one-way ANOVA) was used to compare data among multiple groups. The LSD is chosen when the variance is uniform, and Brown-Forsythe and Welch ANOVA tests are chosen when the variance is not uniform. The difference was statistically significant at $P < 0.05$.

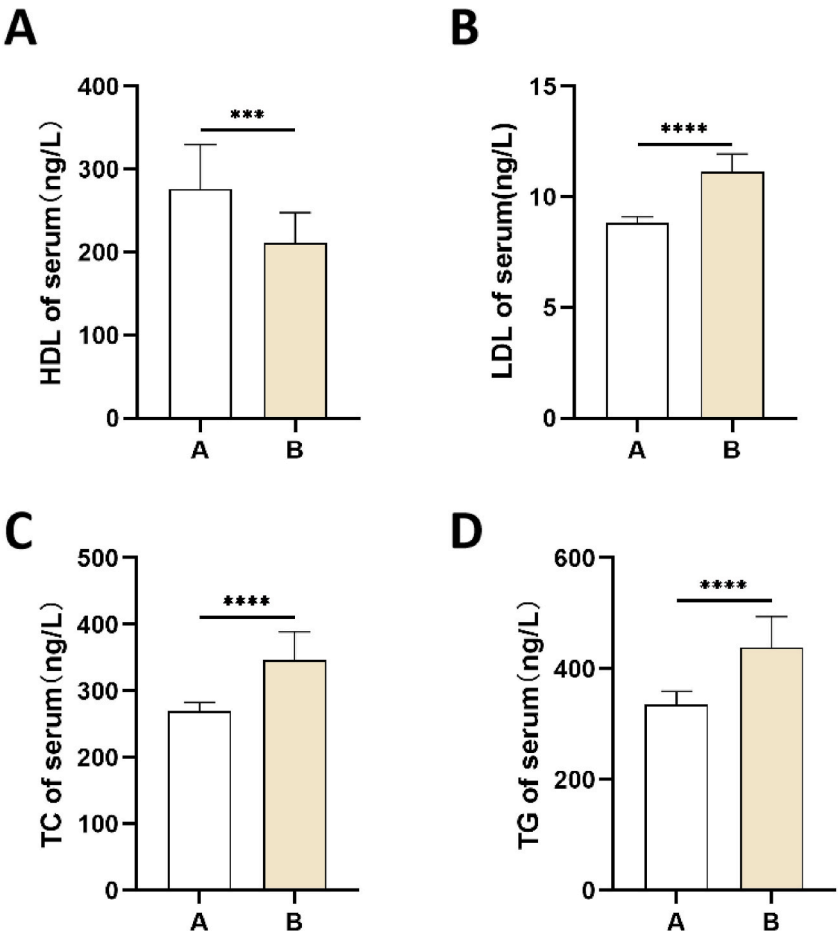

Fig. 3. Preparation of the rat model of hyperlipidemia. Blood lipid levels of rats in group A (n = 6) and group B (n = 24) before intervention. (A) HDL; (B) LDL; (C) TC; (D) TG. Compared with group A in the figure, ***P < 0.001 or ****P < 0.0001.

3. Experimental results

3.1. Evaluation of hyperlipidemia induction model

As shown in Fig. 3, the data of LDL, TC, TG, and HDL levels of rats in group A (n = 6) and group B (n = 24) are normally distributed within the group, and the difference within the group is not statistically significant ($P > 0.05$). The serum HDL (Fig. 3(A), t = −5.757, df = 28) level of rats decreases, while LDL (Fig. 3(B), t = −6.826, df = 28), TC (Fig. 3(C), t = −7.556, df = 26.218), and TG (Fig. 3(D), t = −6.802, df = 20.544) levels increase in group B compared with group A, and the difference is statistically significant ($P < 0.001$). Therefore, the rat hyperlipidemia model was established successfully. The 24 rats in group B were then randomly divided into the HFD group, HFD + Statin group, HFD + Moxi group, and HFD + CC + Moxi group (n = 6). Moreover, rats were observed and given different interventions.

3.2. Grain-sized moxibustion improves the blood lipid level in hyperlipidemic rats

The serum levels of HDL, LDL, TC, and TG after 10 weeks of intervention in each group are shown in Fig. 4. Compared with the Blank group, the HFD group shows a decreased HDL (Fig. 4(A), t = 5.824, df = 9.824, and $P < 0.01$) and increased LDL (Fig. 4(B), t = 8.433, df = 7.726, and $P < 0.001$), TC (Fig. 4(C), q = 17.97, df = 25, and $P < 0.0001$), and TG (Fig. 4(D), q = 16.34, df = 25, and $P < 0.0001$). Compared with the HFD group, the HFD + Moxi group exhibits decreased serum LDL (Fig. 4(B), t = 4.831, df = 9.910, and P

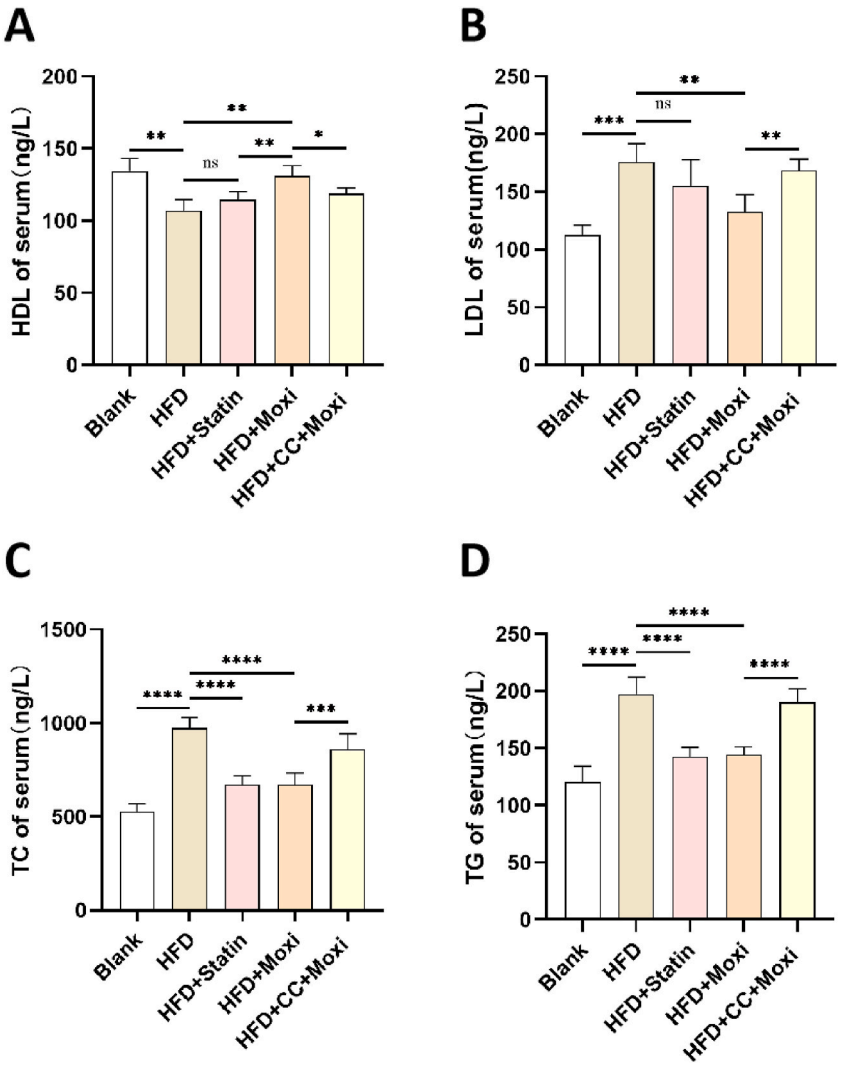

Fig. 4. Blood lipid level of SD rats in each group after intervention. After the intervention cycle, the blood lipid level of rats in each group (n = 6). (A) HDL; (B) LDL; (C) TC; (D) TG. Each group of data accords with normal distribution. Compared with the selected group, $^{*}P < 0.05$, $^{**}P < 0.01$, $^{***}P < 0.001$ or $^{****}P < 0.0001$.

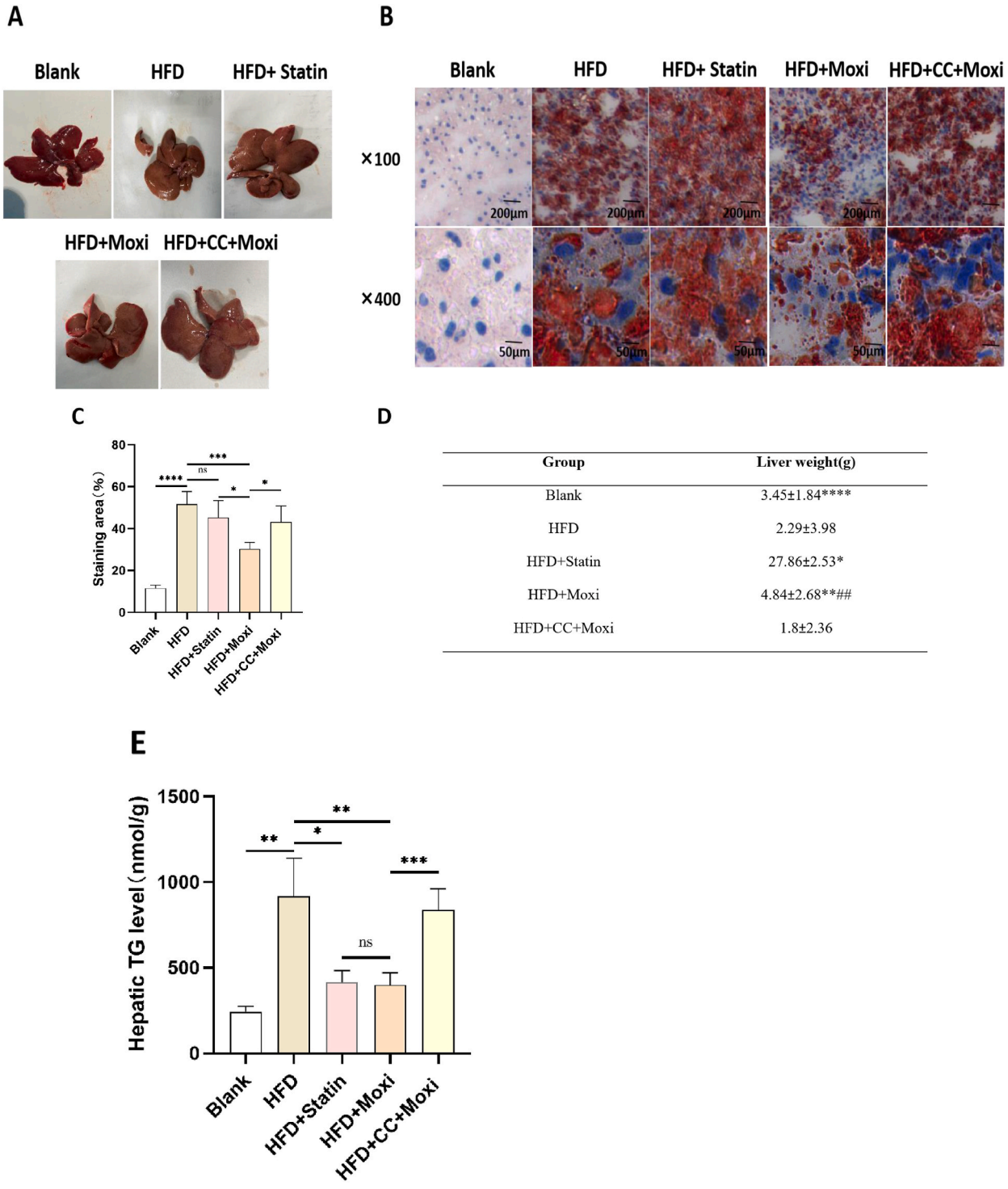

Group	Liver weight(g)
Blank	3.45±1.84****
HFD	2.29±3.98
HFD+Statin	27.86±2.53*
HFD+Moxi	4.84±2.68**##
HFD+CC+Moxi	1.8±2.36

Fig. 5. Liver lipid deposition of SD rats after the intervention. Lipid deposition in the liver of hyperlipidemic rats was determined by ORO staining (three independent experiments were conducted for each sample) (n = 6). (A) Typical liver pictures of rats in each group; (B) Liver oil red staining (×100, 400); (C) Analysis of oil red staining area of rats in each group; (D) The average weight of the liver of the rats in each group; (E) Hepatic TG levels measured using the colorimetric method. Compared with the selected group, $^{*}P < 0.05$, $^{**}P < 0.01$, $^{***}P < 0.001$ or $^{****}P < 0.0001$; (D) Compared with the HFD group: $^{*}P < 0.05$, $^{**}P < 0.01$, $^{****}P < 0.0001$; compared with the HFD + CC + Moxi group: $\#\#P < 0.01$. (For interpretation of the references to color in this figure legend, the reader is referred to the Web version of this article.)

< 0.01), TC (Fig. 4(C), q = 12.21, df = 25, and $P < 0.0001$), and TG (Fig. 4(D), q = 11.25, df = 25, and $P < 0.01$) and increased HDL (Fig. 4(A), t = 5.783, df = 9.907, and $P < 0.01$) in SD rats. Compared with the HFD + Statin group shows significantly decreased serum TC (Fig. 4(C), q = 12.18, df = 25, and $P < 0.0001$) and TG (Fig. 4(D), q = 11.67, df = 25, and $P < 0.0001$) levels, decreased LDL (Fig. 4(B), t = 1.825, df = 8.988, and $P > 0.05$) expression, and increased HDL (Fig. 4(A), t = 1.954, df = 9.234, and $P > 0.05$), but the difference is not statistically significant. Compared with the HFD + Statin group, the increase of serum HDL of SD rats in the HFD + Moxi group is significantly different (Fig. 4(A), t = 5.783, df = 9.907, and $P < 0.01$), and decreased LDL (Fig. 4(B), t = 1.997, df = 8.517, and $P > 0.05$) and, TC (Fig. 4(C), q = 4.644, df = 25, and $P > 0.05$) levels, and increased TG (Fig. 4(D), q = 0.4203, df = 25, and $P > 0.05$), but the difference is not statistically significant. The levels of HDL (Fig. 4(A), t = 3.845, df = 7.969, and $P < 0.05$), LDL (Fig. 4(B), t = 5.043, df = 8.553, and $P < 0.01$), TC (Fig. 4(C), q = 7.567, df = 25, and $P < 0.001$), and TG (Fig. 4(D), q = 9.746, df = 25, and $P < 0.001$) in the HFD + Moxi group are higher than those of the HFD + CC + Moxi group, with statistically significant differences.

The data show that hyperlipidemia can cause a significant decrease in serum HDL and an increase in LDL, TC, and TG in rats, while intragastric administration of atorvastatin and bilateral ST36 grain-sized moxibustion stimulation can increase the serum HDL expression and decrease the serum LDL, TC, and TG expression. Compared with intragastric administration of atorvastatin, grain-sized moxibustion stimulation can increase the serum HDL expression, while the injection of Compound C can affect the improvement of blood lipid in rats by grain-sized moxibustion (Fig. 4).

3.3. *Grain-sized moxibustion improves hepatic steatosis in hyperlipidemic rats*

The liver morphology, weight, ORO staining results, and hepatic TG levels of rats after the intervention cycle in each group are shown in Fig. 5. The liver of the Blank group is reddish-brown, with a soft texture, normal size, low weight, and a low hepatic TG level (Fig. 5(A)(D)(E)), and the ORO staining of this group of samples occasionally shows dispersed lipid droplets without fatty degeneration of hepatocytes (Fig. 5(B)). The livers of the HFD group, HFD + Statin group, HFD + Moxi group, and HFD + CC + Moxi group are white, with liver hypertrophy and weight gain as well as relatively high TG levels due to excessive accumulation of fat in hepatocytes (Fig. 5(A)(D)(E)). Additionally, the ORO staining of HFD group samples shows serious fat changes in liver tissues and hepatocytes, with fat droplets in hepatocytes and different staining depths of ORO (Fig. 5(B)). Compared with the Blank group, the HFD group has greater

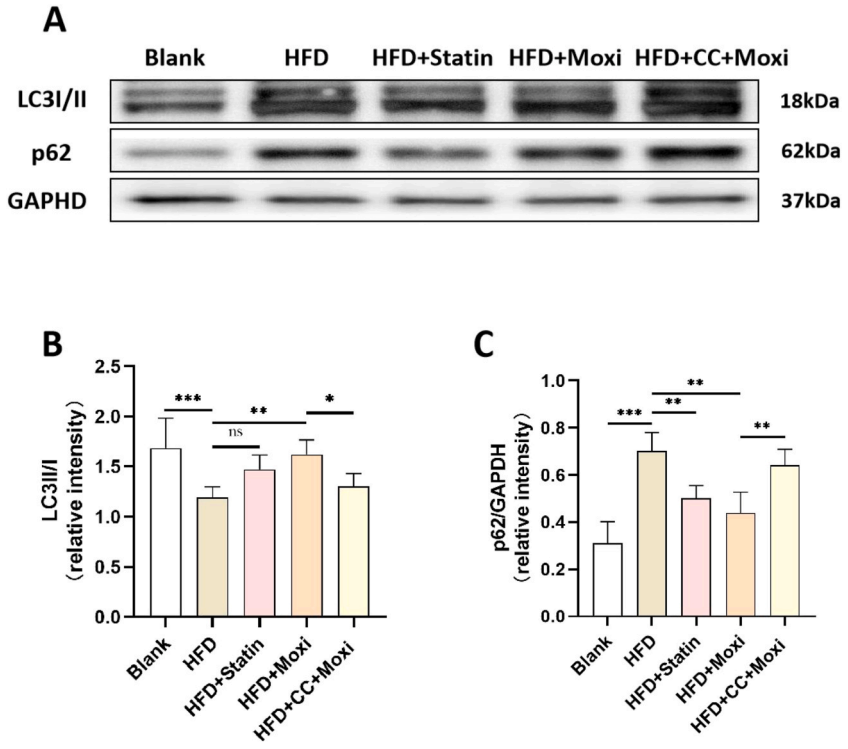

Fig. 6. Expression of LC3I, LC3II, and p62 in the liver of SD rats after the intervention. The expression of LC3I, LC3II, and p62 in the liver of SD rats was detected by WB and IFT (n = 6). The data were expressed as the mean standard deviation of three independent experiments. (A) Protein expression of LC3I, LC3II, and p62 in the liver of rats in each group (supplementary material: Fig. S6(A)-LC3I II; Fig. S6(A)-p62; Fig. S6(A)-GAPDH); (B) Gray value of LC3II/I protein expression in the liver of rats in each group; (C) Gray value of the p62 protein expression in the liver of rats in each group; (D) Immunofluorescence expression of LC3 in the liver of rats in each group; (E) LC3 immunofluorescence nuclear count of rat liver in each group; (F) Immunofluorescence expression of p62 in the liver of rats in each group; (G) p62 immunofluorescence nuclear count of rat liver in each group. Compared with the marked group in the figure, $^{*}P < 0.05$, $^{**}P < 0.01$. $^{***}P < 0.001$ or $^{****}P < 0.0001$.

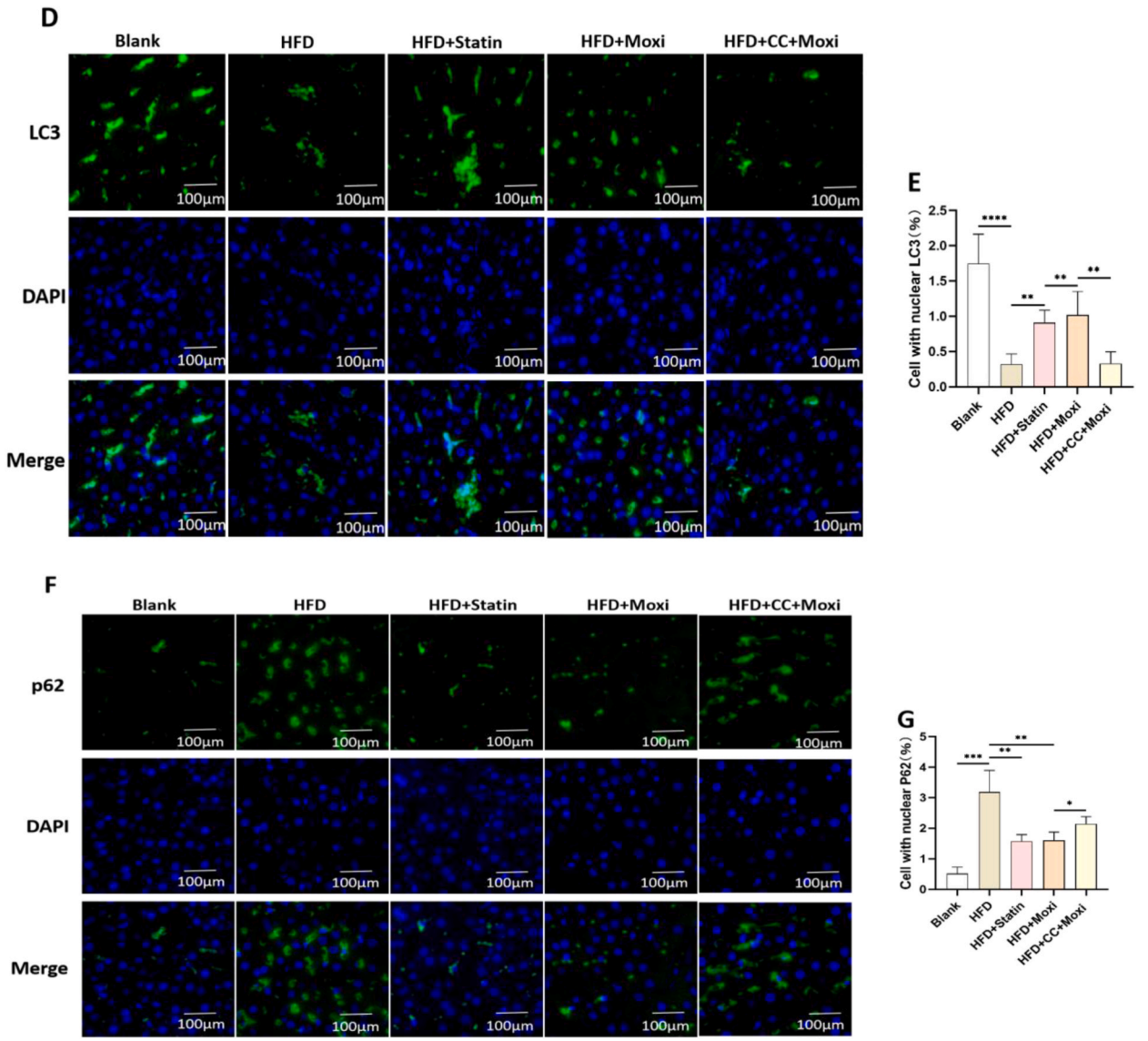

Fig. 6. (*continued*).

weight (q = 16.05, df = 25, and $P < 0.0001$) and larger oil red staining area of the liver (t = 15.94, df = 5.571, and P < 0.001) as well as higher TG levels (t = 7.271, df = 5.188, and P < 0.01), and the difference in weight and oil red staining area between the two groups is extremely significant. Compared with the HFD group, moxibustion improves the steatosis of liver cells, reduces liver weight (HFD + Moxi group: q = 6.343, df = 25, and $P < 0.01$), and significantly reduces the staining area of liver ORO (HFD + Moxi group: t = 7.747, df = 7.562, and P < 0.01) as well as hepatic TG levels (t = 5.380, df = 5.95, and P < 0.01) (Fig. 5(C)(D)(E)). When rats in the HFD + CC + Moxi group are given grain-sized moxibustion with the same frequency and cycle, the weight of the liver (q = 5.929, df = 25, and P < 0.01), the stained area of ORO (t = 3.784, df = 6.629, and P < 0.05) and TG levels (t = 7.486, df = 7.830, and P < 0.001) in this group decrease compared with those in the HFD + Moxi group, and the differences are statistically significant (Fig. 5(B)(C)(D)(E)). The results show that a high-fat diet can significantly increase liver weight, hepatic TG levels, fat deposition in liver tissue, and fatty degeneration of hepatocytes, while atorvastatin and grain-sized moxibustion reduce hepatic TG levels, fat accumulation in liver slices, and fatty degeneration of cells (Fig. 5(B)(C)(E)). Injection of HFD + CC + Moxi can affect the improvement of fatty degeneration of hepatocytes and hepatic TG levels by grain-sized moxibustion.

3.4. Grain-sized moxibustion regulates the expression and distribution of LC3 and p62 in the liver tissue of hyperlipidemic rats

After the intervention, the IFT and WB results of liver LC3 and p62 of rats in each group are shown in Fig. 6. The nucleus of DAPI stained by IFT is blue, and the positive expression of fluorescence is green.

WB and IFT results revealed that compared with the Blank group, the liver of the HFD group shows decreased LC3 level ($q = 6.851$, $df = 25$, and $P < 0.001$, Fig. 6(A)(B); $q = 12.99$, $df = 25$, and $P < 0.0001$, Fig. 6(D)(E)) and increased p62 level ($t = 7.987$, $df = 9.795$, and $P < 0.001$, Fig. 6(A)(C); $t = 8.924$, $df = 5.861$, and $P < 0.001$, Fig. 6(F)(G)). The liver WB detection of rats in the HFD + Statin and

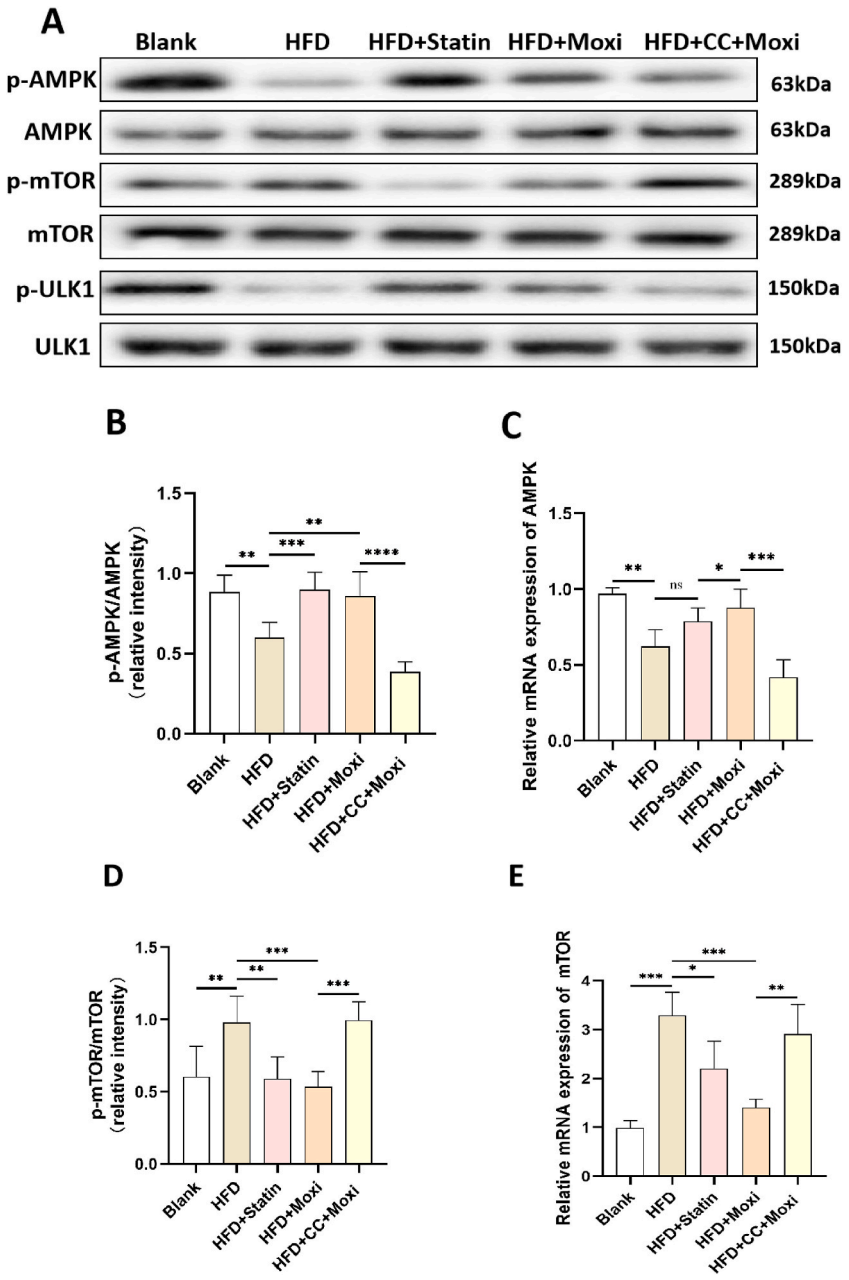

Fig. 7. Expression of p-AMPK,p-mTOR,p-ULK1, and TFEB protein and mRNA in the liver of rats after the intervention. The expression of p-AMPK, p-mTOR, and p-ULK1 in SD rat liver was detected by WB and qPCR, and the expression of TFEB was detected by IHC, IFT, WB, and qPCR (n = 6). The data are expressed as the mean and standard deviation of three independent experiments. (A) Protein expression of p-AMPK, AMPK,p-mTOR, mTOR, p-ULK1, and ULK1 in the liver of rats in each group (supplementary material: Fig. S7(A)-p-AMPK; Fig. S7(A)-AMPK; Fig. S7(A)-p-mTOR; Fig. S7(A)-mTOR; Fig. S7(A)-p-ULK1; Fig. S7(A)-ULK1); (B)(D)(F) Gray value of p-AMPK, p-mTOR, and p-ULK1 protein expression in the liver of rats in each group; (C)(E)(G) AMPK, mTOR, and ULK1 mRNA expression in the liver of rats in each group; (H) Protein expression of cytosol and nuclear TFEB in the liver of rats in each group (supplementary material: Fig. S7(H)-Cytosol TFEB; Fig. S7(H)-GAPDH; Fig. S7(H)-nuclear TFEB; Fig. S7(H)-PCNA); (I) (J) Gray value of cytosol and nuclear TFEB protein expression in the liver of rats in each group; (K) TFEB mRNA expression in the liver of rats in each group; (L) Typical IHC pictures of TFEB in the liver of rats in each group (×100, 200); (M) IHC positive cell count of TFEB in the liver of rats in each group; (N) IFT representative pictures of TFEB in the liver of rats in each group; (O) IF nuclear count of TFEB in the liver of rats in each group. Compared with the marked group in the figure, $*P < 0.05$, $**P < 0.01$, $***P < 0.001$, or $****P < 0.0001$.

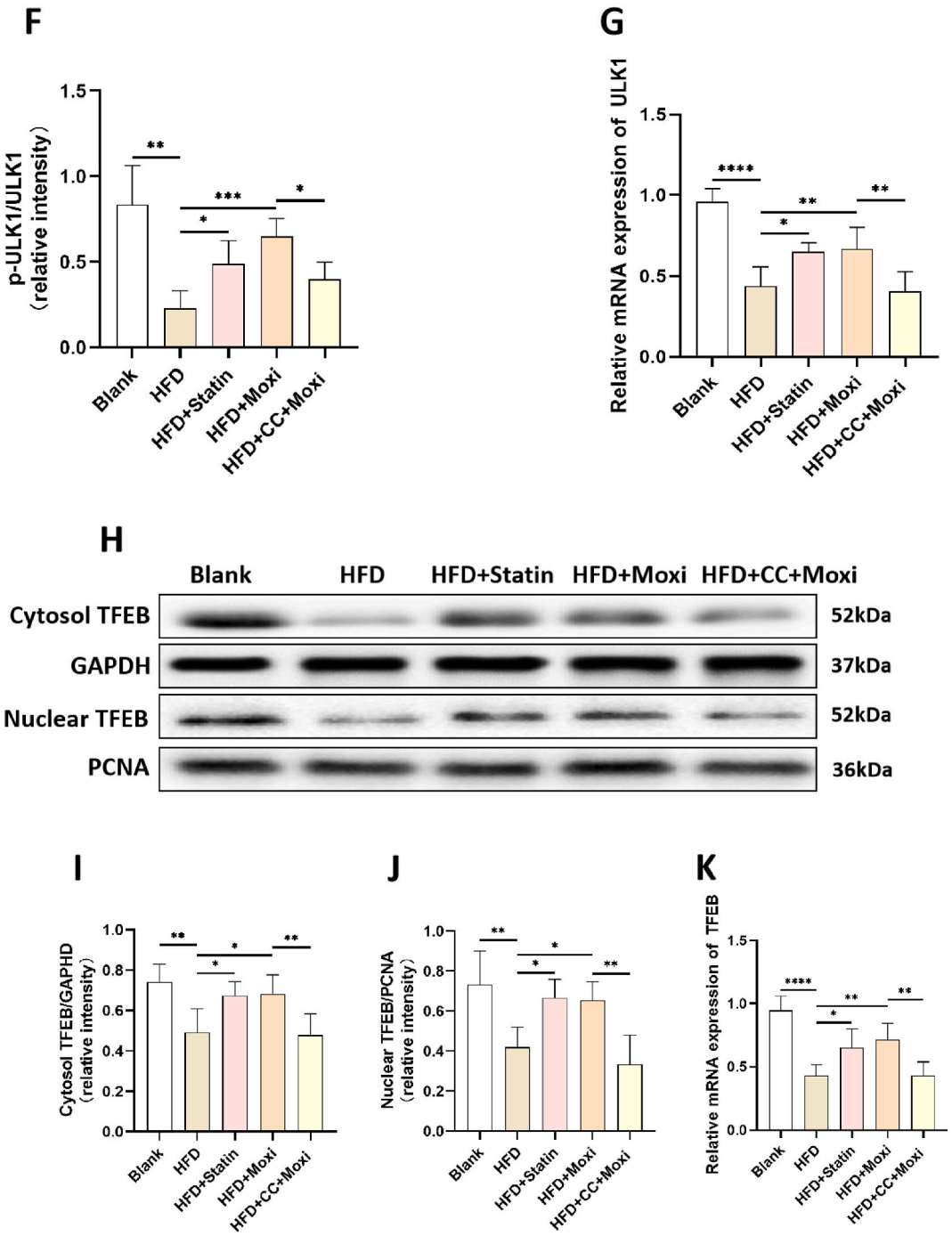

Fig. 7. (*continued*).

HFD + Moxi groups also conforms to the trend of the increasing LC3 ($q = 3.917$, $df = 25$, and $P > 0.05$, Fig. 6(A)(C); $q = 5.989$, $df = 25$, and $P < 0.01$, Fig. 6(A)(B)) expression level and decreasing p62 ($t = 5.189$, $df = 8.879$, and $P < 0.01$, Fig. 6(A)(C); $t = 5.470$, $df = 9.858$, and $P < 0.01$, Fig. 6(A)(C)) expression level compared with that in the HFD group. The WB results were confirmed by IFT analysis ($q = 5.343$, $df = 25$, and $P < 0.01$, Fig. 6(A)(C); $q = 6.351$, $df = 25$, and $P < 0.01$, Fig. 6(A)(B); $t = 5.380$, $df = 5.940$, and $P < 0.01$, Fig. 6(A)(C); $t = 5.165$, $df = 6.480$, and $P < 0.01$, Fig. 6(A)(C)). Compared with the HFD + Moxi group, the HFD + CC + Moxi group shows a decrease in the number of positive nuclei of LC3 ($q = 6.265$, $df = 25$, and $P < 0.01$) and the expression of the gray value of LC3II/I ($q = 4.502$, $df = 25$, and $P < 0.05$) (Fig. 6(B)(D)(E)), and an increase in the number of positive nuclei and gray values for p62 ($t = 3.686$, $df = 9.787$, and $P < 0.05$; $t = 4.553$, $df = 9.265$, and $P < 0.01$) (Fig. 6(C)(F)(G)).

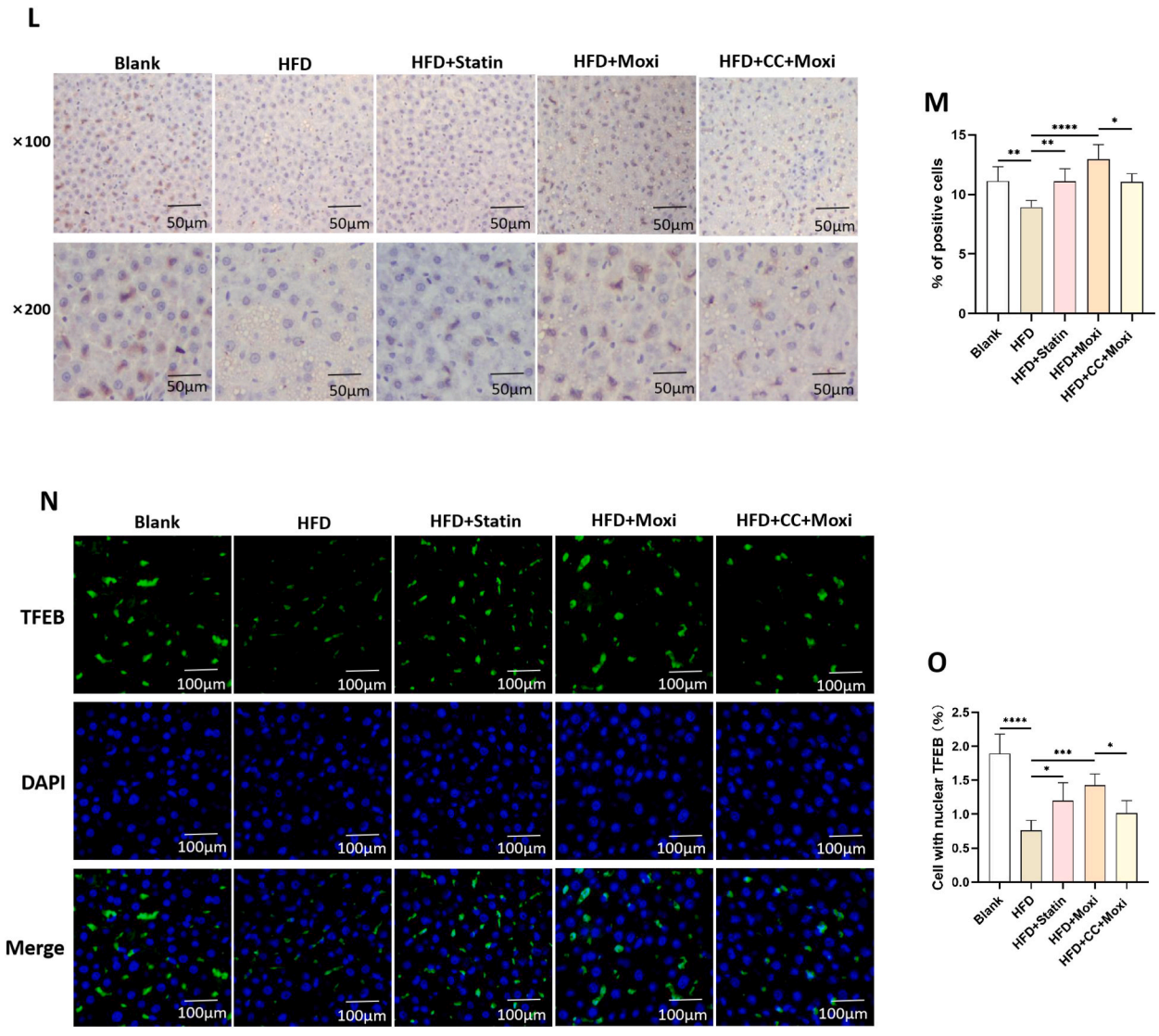

Fig. 7. (*continued*).

The experimental results show that a high-fat diet can reduce the autophagy level of the liver in rats; intragastric administration of atorvastatin and ST36 grain-sized moxibustion stimulation can significantly increase the autophagy level of liver cells, while injection of Compound C inhibitor can affect the increase of autophagy level of liver cells by grain-sized moxibustion.

3.5. Moxibustion regulates the expression distribution of AMPK, mTOR, ULK1, and TFEB and the expression of protein and mRNA in the liver tissue of hyperlipidemic rats

After the intervention, the results of WB, qPCR, IFT, and IHC of AMPK, mTOR, ULK1, and TFEB in the liver of rats in each group are shown in Fig. 6. In the IFT picture, the detected DAPI-stained nucleus is blue, and the positive expression of fluorescence is green. However, in IHC pictures, the hematoxylin-stained nucleus is blue, and diaminobenzidine (DAB) shows a positive expression of brown-yellow.

The results of WB and qPCR show that the expression of p-AMPK decreases ($q = 6.387$, $df = 25$, and $P < 0.01$, Fig. 7(A)(B); $t = 7.308$, $df = 6.255$, and $P < 0.01$, Fig. 7(C)), the expression of p-mTOR increases ($q = 5.824$, $df = 25$, and $P < 0.01$, Fig. 7(A)(D); $t = 11.44$, $df = 6.059$, and $P < 0.001$, Fig. 7(E)), the expression of p-ULK1 decreases ($t = 5.975$, $df = 6.931$, and $P < 0.01$, Fig. 7(A)(F); $q = 11.98$, $df = 25$, and $P < 0.0001$, Fig. 7(G)), the expression of cytosol and nuclearTFEB decreases ($q = 6.377$, $df = 25$, and $P < 0.01$, $q = 6.214$, $df = 25$, and $P < 0.01$, Fig. 7(H)(I)(K); $q = 10.67$, $df = 25$, and $P < 0.0001$, Fig. 7(H)(J)) in the HFD group compared with the Blank group. Compared with the HFD group, HFD + Stain and HFD + Moxi groups show an increased p-AMPK expression (Fig. 7(A)(B)(C)), a decreased p-mTOR expression (Fig. 7(A)(D)(E)), an increased p-ULK1 expression (Fig. 7(A)(F)(G)) and an increased nuclear

TFEB expression. The western blot and qPCR expression of p-AMPK ($q = 5.824$, $df = 25$, and $P < 0.01$; $t = 3.831$, $df = 9.895$, and $P < 0.05$), p-mTOR ($q = 6.904$, $df = 25$, and $P < 0.001$; $t = 9.248$, $df = 6.290$, and $P < 0.001$), p-ULK1 ($t = 7.051$, $df = 9.992$, and $P < 0.001$; $q = 5.228$, $df = 25$, and $P < 0.01$), cytosol and nuclear TFEB ($q = 4.888$, $df = 25$, and $P < 0.05$; $q = 4.619$, $df = 25$, and $P < 0.05$; $q = 5.866$, $df = 25$, and $P < 0.01$) in the HFD + Moxi group is significantly different from that in the HFD group. Western blot and qPCR results suggest that compared with the HFD group, the HFD + Statin group has increased expressions of hepatic p-AMPK ($q = 6.777$, $df = 25$, and $P < 0.001$; $t = 2.891$, $df = 9.561$, and $P > 0.05$), p-ULK1 ($t = 3.803$, $df = 9.317$, and $P < 0.05$; $q = 4.849$, $df = 25$, and $P < 0.05$), and cytosol and nuclear TFEB ($q = 4.621$, $df = 25$, and $P < 0.05$; $q = 4.833$, $df = 25$, and $P < 0.05$; $q = 4.622$, $df = 25$, and $P < 0.05$), and decreased p-mTOR ($q = 6.033$, $df = 25$, and $P < 0.01$; $t = 3.642$, $df = 9.669$, and $P < 0.05$) expression ($P < 0.05$). Compared with the results of liver western blot and qPCR in the HFD + Moxi group, those in the HFD + CC + Moxi group show that the p-AMPK ($q = 10.69$, $df = 25$, and $P < 0.0001$; $t = 6.751$, $df = 9.957$, and $P < 0.0001$) expression decreases, p-mTOR ($q = 7.113$, $df = 25$, and $P < 0.001$; $t = 5.835$, $df = 5.778$, and $P < 0.01$) expression increases, p-ULK1 expression decreases ($t = 4.253$, $df = 9.966$, and $P < 0.05$; $q = 5.949$, $df = 25$, and $P < 0.01$), cytosol and nuclear TFEB expression decreases ($q = 5.267$, $df = 25$, and $P < 0.01$; $q = 6.305$, $df = 25$, and $P < 0.01$; $q = 5.829$, $df = 25$, and $P < 0.01$).

The results of IHC and IFT show that the number of positive nuclei and positive cell count of TFEB in the liver of the HFD group decreases compared with that of the Blank group ($q = 5.407$, $df = 25$, and $P < 0.01$, Fig. 7(L)(M); $q = 12.77$, $df = 25$, and $P < 0.0001$, Fig. 7(N)(O)). The number of positive nuclei and positive cells in liver TFEB increases in the HFD + Stain and HFD + Moxi groups compared with the HFD group. Specifically, the number of TFEB-positive cells in the liver of the HFD + Stain group is significantly different from that of the HFD group ($q = 5.335$, $df = 25$, and $P < 0.01$, Fig. 7(M); $q = 4.891$, $df = 25$, and $P < 0.05$, Fig. 7(O)); the number of TFEB-positive cells and nuclei in the liver of the HFD + Moxi group is significantly different from that of the HFD group ($q = 9.933$, $df = 25$, and $P < 0.0001$, Fig. 7(M); $q = 7.491$, $df = 25$, and $P < 0.001$, Fig. 7(O)). Compared with the HFD + Moxi group, the HFD + Moxi + CC group shows that the number of TFEB positive cells and positive nuclei in the liver significantly decreases ($q = 4.720$, $df = 25$, and $P < 0.05$, Fig. 7(M); $q = 4.653$, $df = 25$, and $P < 0.05$, Fig. 7(O)).

The experimental results show that a high-fat diet can significantly reduce the p-AMPK, p-ULK1, and TFEB expression in rat liver and increase the p-mTOR expression. Intragastric administration of atorvastatin and ST36 grain-sized moxibustion stimulation can significantly increase the expression of p-AMPK, p-ULK1, and TFEB, while injection of HFD + CC + Moxi can affect the increase in p-AMPK, p-ULK1, and nuclear TFEB expression and the decrease in the p-mTOR expression in rat liver. Moreover, TFEB is an important transcription factor that activates transcription and exerts autophagy. The expression of p-ULK1 and nuclear TFEB is closely related to the level of autophagy. Therefore, the stimulation of grain-sized moxibustion in the ST36 acupoints of rats can significantly improve the reduction of liver autophagy induced by a high-fat diet. The mechanism is related to the increase in the p-AMPK, p-ULK1 expression, and the inhibition of the p-mTOR expression in the liver by grain-sized moxibustion, probably through the AMPK/mTOR pathway.

4. Discussion

Excessive intake of exogenous lipids is an important cause of hyperlipidemia. Dyslipidemia can lead to hepatocyte damage, mainly manifested as steatosis and necrosis of hepatocytes. Liver diseases, such as NAFLD and Nonalcoholic steatohepatitis (NASH), occur with hepatocyte damage, and dyslipidemia is the beginning of a series of subsequent pathological changes [5]. Therefore, taking the hyperlipidemic rat model as the study subject is more consistent with the pathological process of hepatocyte damage caused by dyslipidemia.

In this study, a high-fat-diet induced hyperlipidemia maintained a stable hyperlipidemic state and promoted hepatocellular steatosis. An attempt was made to simulate the disease process in most patients with hepatic steatosis induced by hyperlipidemia. Moxibustion effectively improved dyslipidemia and hepatic lipid accumulation in hyperlipidemic rats and promoted autophagy of hepatocytes. Previous studies have also shown that moxibustion can improve dyslipidemia in hyperlipidemic rats with similar effects on TC and TG as statins [29]. Clinical studies have shown that moxibustion can significantly reduce blood TC, TG, and LDL-C levels in hyperlipidemia patients ($P < 0.01$), suggesting its regulatory effect on dyslipidemia [30]. In our research, we discovered that moxibustion had a greater effect on lipoproteins than triglycerides and was capable of reducing levels of serum LDL while increasing HDL levels. We postulated that this might be due to the antioxidative and anti-inflammatory effects of moxibustion, which may improve the lipid environment by ameliorating oxidative stress and inflammation [31–33]. Lipoproteins serve the function of regulating serum lipids, while triglycerides are merely a product of this process. From this perspective, we suggest that moxibustion may improve the system that regulates serum lipids rather than targeting a specific product. Numerous studies have demonstrated the cholesterol-lowering effects of moxibustion on serum LDL [23,34–37], while some studies suggest that moxibustion has no statistically significant effect on serum HDL [23,38]. We attribute this discrepancy to differences in moxibustion acupoints and treatment duration, as well as metabolic variations between animals and humans. Studies have shown that moxibustion can increase serum HDL-C levels and decrease LDL-C levels [39]. The aforementioned studies suggest that the mechanisms underlying the effects of moxibustion on blood lipids and hepatic steatosis are still complex and require further investigation and contemplation. However, it is indeed evident that moxibustion does have an impact on serum lipoproteins.

During the autophagy of hepatocytes, LC3 is the most widely used autophagy marker that modifies autophagy with its fatty form LC3II participating in the mechanism of phagocytic cell membrane expansion and autophagy biological formation [15,40] p62 is a substrate connecting LC3 and ubiquitination [41]and interacts with LC3 to provide autophagy degradation selectivity [42]. In the autophagy process, LC3 integrates into the autophagosome after interacting with p62 and is degraded in the autophagy-lysosome [43]. Additionally, TFEB can bind to the promoter region of the target gene to initiate the transcription of autophagy-related genes and the

synthesis of lysosomes [38]. This study revealed that moxibustion could regulate hepatocyte autophagy by increasing LC3 expression and decreasing p62 expression. The WB and IFT results of LC3 and p62 in the study were not completely consistent, possibly due to the complex results of the WB test and the variation in variable solubility [44].

The activation of AMPK is related to ATP, ADP, and AMP and can phosphorylate TSC2 and RAPTOR and then down-regulate mTOR [45]. Additionally, mTOR can directly phosphorylate TFEB, regulate the c-terminal serine structure of TFEB to phosphorylate it, affect the transposition of TFEB, and play a role in the generation stage of the lysosome [46]. The regulation of autophagy by TFEB is mainly achieved by dephosphorylation. When mTOR is inhibited, mTORC1 dissociates from the lysosome, and TFEB separates from cytoplasmic molecular chaperone 14-3-3 to dephosphorylate into the nucleus and combine with the promoter region of the target gene, which initiates the transcription of LC3 autophagy gene and lysosome synthesis [46]. Therefore, TFEB is isolated in the cytoplasm. Once activated, it can translocate to the nucleus, coordinate the expression and regulation of lysosome, and participate in the gene transcription process of autophagy-lysosome (represented by LC3-TFEB) [46]. In addition, the serine/threonine kinase ULK-1 may be phosphorylated by AMPK and mTOR to regulate autophagy14. Liu et al. found that hepatocyte autophagy in HFD mice could be repaired by restoring AMPK/mTOR/ULK1-mediated autophagy [47].

Moxibustion can activate AMPK by affecting ATP in mice and rats [48,49]. Moxibustion can effectively improve the ATP level, change the energy in local and diseased areas of moxibustion in a chronic disease state, activate the AMPK expression, and stimulate a series of reactions downstream of the pathway [46,50]. In this study, Compound C was adopted to inhibit AMPK, and WB and qPCR methods were used to detect the expression of p-AMPK, p-mTOR, p-ULK1 protein, and mRNA in rat liver tissues. The expression of proteins related to the AMPK/mTOR pathway was found to change significantly. However, the stimulation of grain-sized moxibustion in ST36 can significantly increase the expression of p-AMPK, p-ULK1, and nuclear TFEB in the liver of hyperlipidemic rats and inhibit the expression of p-mTOR. The activation of the AMPK/mTOR signal pathway and the expression of p-ULK1 and TFEB in rat liver were significantly affected by grain-sized moxibustion after Compound C injection, indicating that the increased p-ULK1 and TFEB expression in hepatocytes by grain-sized moxibustion was achieved by activating the AMPK/mTOR signaling pathway.

The biological effects of moxibustion include local effects mainly consisting of skin, muscle, and joint, superficial vascular effects, remote effects mainly composed of distal vascular and visceral effects, and systemic effects mainly composed of the neuroendocrine-immune network [18]. Moreover, the biological effect of moxibustion is closely related to the moxibustion site, the temperature of moxibustion, the number of moxibustion sessions, and the frequency and duration of moxibustion treatment, etc. [21,33]. Therefore, the biological effect of moxibustion should include three elements: the corresponding pathological state, specific stimulation site, and appropriate moxibustion parameters. The effect of ST36 acupoints moxibustion on the liver is caused by giving ST36 acupoints moxibustion stimulation with the corresponding temperature and intensity of the related pathological process of the liver. Several studies have focused on the effects of moxibustion on blood lipids and liver. L. Duan et al. [35] found that crude-herb moxibustion can improve hepatic steatosis in rats fed with a high-fat diet, Liu Xia et al. [51] found that partitioned moxibustion can increase the expression of liver X receptor alpha (LXRα), which is involved in regulating blood lipids and hepatic lesions by promoting cholesterol efflux from the liver. In addition, moxibustion has been shown to improve the serum levels of aspartate aminotransferase (AST) and alanine aminotransferase (ALT) in the Hepa1-6 mouse model of liver cancer [52]. In animal models, moxibustion has been shown to affect the function of liver cells by regulating levels of hepatic glycogen, insulin, glycerol, xanthine, adenosine, lysine, niacin, superoxide dismutase (SOD), malondialdehyde (MDA), catalase (CAT), and glutathione peroxidase (GSH-Px) [34].

Although the rat model of hyperlipidemia is taken as the research object, this research pays attention to the repair effect of moxibustion on liver cells due to the relationship between dyslipidemia and liver metabolic diseases, which is also in line with the diagnosis and treatment idea of "treating diseases before treatment" in Chinese medicine.

There should be a complete path from ST36 moxibustion to the target organ response to trigger the effect. Studies have shown that moxibustion at 46 °C can change glucose, lactic acid, pyruvic acid, and glutamic acid in local tissue microdialysis solution and can also promote the cycle of tricarboxylic acid and affect the energy metabolism of the body [53]. In addition, moxibustion at ST36 at 40 °C can cause hypomethylation of CG sequence in the local skin of rats, and the functional classification of hypomethylation genes mainly regulates mitochondrial autophagy, immunity and anti-inflammation, blood circulation, and other biological processes [54]. Moxibustion at ST36 acupoint at a specific temperature can affect not only the energy metabolism of local tissues and related viscera but also the initial stage of transcription to play a specific biological role. In the local area of moxibustion, thermal stimulation may promote mast cell degranulation [55]. In addition, moxibustion above 45 °C can activate TRPV1 in the ST36 acupoint to make TRPV1 in the spinal dorsal horn respond, thus realizing the effect mechanism of moxibustion "promoting circulation by warming" and "regulating fat and dredging pulse" [56,57]. When the moxibustion temperature falls below 40°C, the effect is invalid, while a valid moxibustion temperature is above 45°C due to its ability to activate not only C-type nociceptor receptors but also TRPV1 receptors [58,59]. Studies have shown that the initiation of the moxibustion warming effect involves the activation of specific receptors, Langerhans cells, and heat shock proteins at acupoints, inducing a variety of local effects [60], such as promoting the wound healing process [61], joint pain relief [62] and affecting superficial vessels [63]. Then, through nerve and body fluid pathways, moxibustion warming stimulation signals and follow-up effects are transmitted to distant organs and the whole body, causing follow-up effects on distant specific target organs and the whole body system [21]. The production of the moxibustion effect is complex. The effective volatile chemical components of Artemisia argyi, including 1,8-cineole enhancement, can activate thermosensitive channels TRPV1, TRPA1, and TPRM8, while camphor and eugenol are activators of TRPV1, TRPA1, and TRPV3 [64]. Furthermore, the production of the moxibustion effect should be comprehensively considered in conjunction with the occurrence of pathological conditions. In disease models, acupoints exhibit sensitization, the substance basis of which is the formation of an "acupuncture sensitization pool" in the local microchemical environment under the action of harmful stimulation, including TRPV1, 5-hydroxytryptamine, histamine, and other biologically active substances [65,66], which may be the material basis for the generation of moxibustion effect.

Based on previous studies focusing on the local energy metabolism of ST36 acupoint, this study further investigated the activation of the AMPK/mTOR pathway of liver energy metabolism after moxibustion to promote the autophagy of hepatocytes. Therefore, moxibustion at ST36 can activate the AMPK/mTOR pathway in the liver and up-regulate ULK1 and nuclear TFEB expression, thus promoting autophagy of liver cells, which may be a potential pathway of the effect of moxibustion at ST36 on the liver from a metabolic perspective (Fig. 8).

Moxibustion is safe and effective to some extent as a complementary therapy for hyperlipidemia patients. In contrast, there is also a debate over whether moxibustion has therapeutic effects or merely warming ones. It is important to understand the mechanism of moxibustion by understanding the specifics of moxibustion temperature. Making sure that the effects of moxibustion are not just warming is important for developing moxibustion in the treatment of hyperlipidemia. Moxibustion's effects on hepatic lipid accumulation and dyslipidemia and related tissues, cells, and signal pathways must be objectively investigated to dispel these doubts. As is known to all, obtaining human tissues or cells is unethical and prohibited. For this reason, animal studies of moxibustion for hyperlipidemia are valuable and cannot be entirely replaced by clinical trials. Thus, we performed animal experiments to explore the effect of moxibustion on hepatocellular autophagy in rats with hyperlipidemia. In the research related to moxibustion, researchers have paid more attention to the effects generated by moxibustion, but a lack of in-depth and systematic studies on its specific mechanisms. Therefore, it is necessary to employ the knowledge and techniques of molecular biology and systems biology to explore in-depth and investigate suitable paradigms for the study of moxibustion. In the next 5 years, research on the advantageous diseases and underlying mechanisms of moxibustion will be a key focus of this field, which requires the joint effort of both clinical and basic researchers.

4.1. Limitations

In this study, there are some limitations, such as the small number of animals in each group. The research was, however, conducted in accordance with reduction strategies in animal research [67]. Secondly, rats and humans have different metabolic rates, and these differences need to be addressed before our results can be applied to the clinic. As a somatic stimulation, moxibustion has inherent biological properties and pathways to produce visceral effects. In this study, we only explored the role of the AMPK/mTOR signaling pathway in improving hepatocyte autophagy by moxibustion but failed to observe the changes in ATP, ADP, and AMP and the response of hepatocytes to moxibustion from the perspective of energy metabolism. There is a shortage in the exploration of the complete biological pathway of "body surface - viscera" in moxibustion at ST36. In addition, since the HFD + CC group was not set up, the specific role of the AMPK inhibitor Compound C remains unclear.

5. Conclusion

Moxibustion at ST36 can improve the blood lipid level of SD rats with hyperlipidemia, increase the expression of p-ULK1 and nuclear TFEB by activating the AMPK/mTOR signaling pathway, and initiate the transcription of autophagy genes such as LC3 and lysosome synthesis to improve the autophagy level of rat hepatocytes, thus improving the hepatocyte damage and hepatic lipid accumulation.

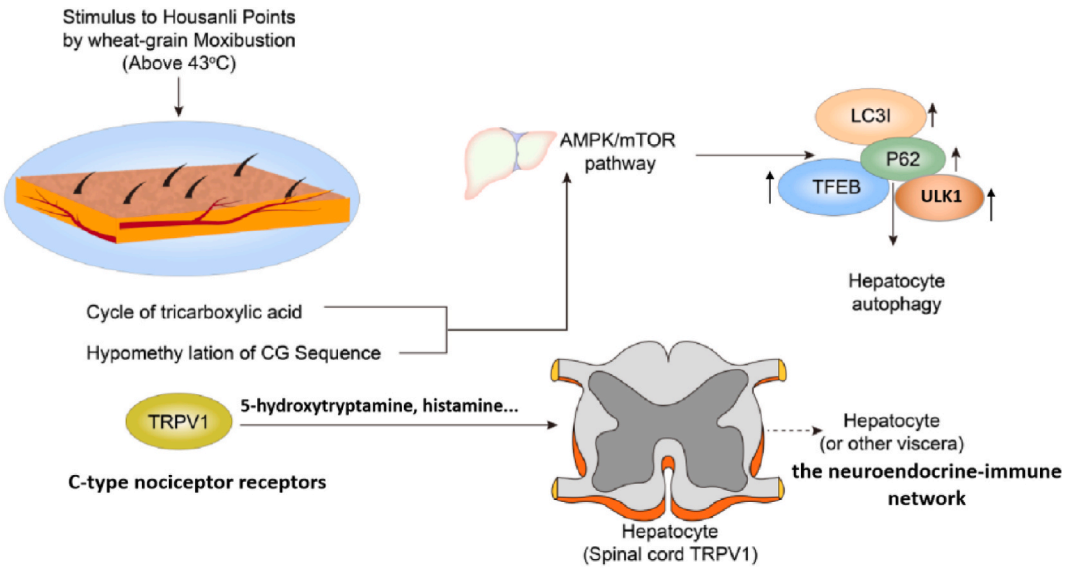

Fig. 8. Possible complete path of the ST36 acupoints moxibustion effect on the liver from the metabolic perspective. → indicates positive regulation relationship; ⇢ indicates the potential regulatory relationship; ↑ indicates the increase of expression; ↓ indicates that the expression decreases.

Author contribution statement

Qian Xu: Conceived and designed the experiments; Performed the experiments; Analyzed and interpreted the data; Wrote the paper.

Huanxi Wu: Performed the experiments; Analyzed and interpreted the data; Wrote the paper.

Haibin Zhu, Chengxuan Lu: Contributed reagents, materials, analysis tools or data; Analyzed and interpreted the data; Performed the experiments.

Jiangjia Tao, Ziqiu Zhou: Performed the experiments.

Jianbin Zhang: Conceived and designed the experiments; Wrote the paper.

Funding statement

Jianbin Zhang was supported by National Natural Science Foundation of China {81973947}

M.D. Qian Xu was supported by Graduate Research and Innovation Projects of Jiangsu Province {KYCX20_1543}

Data availability statement

Data included in article/supplementary material/referenced in article.

Declaration of interest's statement

The authors declare that they have no known competing financial interests or personal relationships that could have appeared to influence the work reported in this paper.

Appendix A. Supplementary data

Supplementary data to this article can be found online at https://doi.org/10.1016/j.heliyon.2023.e15316.

References

[1] C. Gils, A.-S.F. Thorsen, M. Nybo, Lipemia Index and screening for hyperlipidemia - a diagnostic opportunity? Clin. Chim. Acta [Internet] 501 (2020) 83–84, https://doi.org/10.1016/j.cca.2019.10.024.

[2] F. Mansour-Ghanaei, F. Joukar, S.N. Mobaraki, S. Mavaddati, S. Hassanipour, M. Sepehrimanesh, Prevalence of non-alcoholic fatty liver disease in patients with diabetes mellitus, hyperlipidemia, obesity and polycystic ovary syndrome: a cross-sectional study in north of Iran, Diabetes Metab. Syndr. [Internet] 13 (2) (2019) 1591–1596, https://doi.org/10.1016/j.dsx.2019.03.009.

[3] M. Gao, W. Zhao, C. Li, X. Xie, M. Li, Y. Bi, et al., Spermidine ameliorates non-alcoholic fatty liver disease through regulating lipid metabolism via AMPK, Biochem. Biophys. Res. Commun. [Internet] 505 (1) (2018) 93–98, https://doi.org/10.1016/j.bbrc.2018.09.078.

[4] Z. Xu, W. Hu, B. Wang, T. Xu, J. Wang, D. Wei, Canagliflozin ameliorates nonalcoholic fatty liver disease by regulating lipid metabolism and inhibiting inflammation through induction of autophagy, Yonsei Med. J. [Internet] 63 (7) (2022) 619–631, https://doi.org/10.3349/ymj.2022.63.7.619.

[5] J. Hannon Hashim Al-Awadi, H. Rashid, J. Hassen, High fat diet induce hyperlipidemia incidences with sever changes in liver tissue of male albino rats: a histological and biochemical Study, Karbala J. Pharm. Sci. (2013) 21–32.

[6] L. Li, Q. Li, W. Huang, Y. Han, H. Tan, M. An, et al., Dapagliflozin alleviates hepatic steatosis by restoring autophagy via the AMPK-mTOR pathway, Front. Pharmacol. [Internet] 12 (2021), 589273, https://doi.org/10.3389/fphar.2021.589273.

[7] C. Shi, W. Xue, B. Han, F. Yang, Y. Yin, C. Hu, Acetaminophen aggravates fat accumulation in NAFLD by inhibiting autophagy via the AMPK/mTOR pathway, Eur. J. Pharmacol. [Internet] 850 (2019) 15–22, https://doi.org/10.1016/j.ejphar.2019.02.005.

[8] A. Marchetti, M. Rosellini, V. Mollica, A. Rizzo, E. Tassinari, G. Nuvola, et al., The molecular characteristics of non-clear cell renal cell carcinoma: what's the story Morning Glory? Int. J. Mol. Sci. [Internet] 22 (12) (2021) 6237, https://doi.org/10.3390/ijms22126237.

[9] M. Rosellini, A. Marchetti, V. Mollica, A. Rizzo, M. Santoni, F. Massari, Prognostic and predictive biomarkers for immunotherapy in advanced renal cell carcinoma, Nat. Rev. Urol. [Internet] 20 (3) (2023) 133–157, https://doi.org/10.1038/s41585-022-00676-0.

[10] V. Mollica, I. Maggio, A. Lopez-Beltran, R. Montironi, A. Cimadamore, L. Cheng, et al., Combination therapy in advanced urothelial cancer: the role of PARP, HER-2 and mTOR inhibitors, Expert Rev. Anticancer. Ther. [Internet] 20 (9) (2020) 755–763, https://doi.org/10.1080/14737140.2020.1807334.

[11] H. Nakatogawa, Y. Ichimura, Y. Ohsumi, Atg8, a ubiquitin-like protein required for autophagosome formation, mediates membrane tethering and hemifusion, Cell [Internet] 130 (1) (2007) 165–178, https://doi.org/10.1016/j.cell.2007.05.021.

[12] S. Pankiv, T.H. Clausen, T. Lamark, A. Brech, J.-A. Bruun, H. Outzen, et al., P62/SQSTM1 binds directly to Atg8/LC3 to facilitate degradation of ubiquitinated protein aggregates by autophagy, J. Biol. Chem. [Internet] 282 (33) (2007) 24131–24145, https://doi.org/10.1074/jbc.m702824200.

[13] X. Chao, S. Wang, K. Zhao, Y. Li, J.A. Williams, T. Li, et al., Impaired TFEB-mediated lysosome biogenesis and autophagy promote chronic ethanol-induced liver injury and steatosis in mice, Gastroenterology [Internet] 155 (3) (2018) 865–879, https://doi.org/10.1053/j.gastro.2018.05.027, e12.

[14] J. Kim, M. Kundu, B. Viollet, K.-L. Guan, AMPK and mTOR regulate autophagy through direct phosphorylation of Ulk1, Nat. Cell Biol. [Internet] 13 (2) (2011) 132–141, https://doi.org/10.1038/ncb2152.

[15] X. Peng, Y. Yang, L. Tang, J. Wan, J. Dai, L. Li, et al., Therapeutic benefits of apocynin in mice with lipopolysaccharide/D-galactosamine-induced acute liver injury via suppression of the late stage pro-apoptotic AMPK/JNK pathway, Biomed. Pharmacother. [Internet] 125 (110020) (2020), 110020, https://doi.org/10.1016/j.biopha.2020.110020.

[16] J.-B. Zhang, L.-L. Wang, H.-G. Wu, L. Hu, X.-R. Chang, X.-G. Song, et al., Theory study: warming-dredging and warming-reinforcing of moxibustion, Zhongguo Zhen Jiu 32 (11) (2012) 1000–1003.

[17] M.Y. Lim, J. Huang, B. Zhao, Standardisation of moxibustion: challenges and future development, Acupunct. Med. [Internet] 33 (2) (2015) 142–147, https://doi.org/10.1136/acupmed-2014-010688.

[18] K.-Y. Huang, S. Liang, G.-Y. Hu, Y.-Y. Zou, L. Lu, J.-B. Zhang, From biological effects of local cutaneous thermal stimulation to moxibustion therapy, Zhen Ci Yan Jiu 40 (6) (2015) 504–509.

[19] Y. Cui, J. Liu, C. Huang, B. Zhao, Moxibustion at CV4 alleviates atherosclerotic lesions through activation of the LXRα/ABCA1 pathway in apolipoprotein-E-deficient mice, Acupunct. Med. [Internet] 37 (4) (2019) 237–243, https://doi.org/10.1136/acupmed-2016-011317.

[20] X.J. Li, L.H. Kong, G.J. Sun, Effect of suspension moxibustion on the bactericidal effect and inflammatory factor expression of mouse macrophages, J. Hubei Univ. Tradit. Chin. Med. 16 (2) (2014) 14–16.

[21] B. Zhang, Q. Zhao, Y. Li, J. Zhang, Moxibustion alleviates intervertebral disc degeneration via activation of the HIF-1α/VEGF pathway in a rat model, Am. J. Transl. Res. 11 (9) (2019) 6221–6231.

[22] J.M. Zhao, Y.N. Liu, H.D. Zheng, Y. Huang, Q. Qi, H.R. Liu, Effect of herb-partitioned moxibustion on autophagy and immune-associated gene expression profiles in a rat model of crohn's disease, Evid. Based. Complement Alternat. Med. (2019), 3405146.

[23] Q. Li, W. Wang, Q. Ma, R. Xia, B. Gao, G. Zhu, et al., Moxibustion improves chronic heart failure by inhibiting autophagy and inflammation via upregulation of mTOR expression, Evid. Based Complement Alternat. Med. [Internet] 2021 (2021), 6635876, https://doi.org/10.1155/2021/6635876.

[24] J. Roessler, F. Zimmermann, D. Schmidt, U. Escher, A. Jasina, M.M. Heimesaat, et al., Impact of the gut microbiome on the atorvastatin-dependent modulation of the serum lipidome, Eur. Heart J. [Internet] 41 (Supplement_2) (2020), https://doi.org/10.1093/ehjci/ehaa946.3823.

[25] J. Qi, Z. Zhou, C.W. Lim, J.-W. Kim, B. Kim, Amlexanox ameliorates acetaminophen-induced acute liver injury by reducing oxidative stress in mice, Toxicol. Appl. Pharmacol. [Internet] 385 (114767) (2019), 114767, https://doi.org/10.1016/j.taap.2019.114767.

[26] M.-Z. Huang, X.-R. Lu, Y.-J. Yang, X.-W. Liu, Z. Qin, J.-Y. Li, Cellular metabolomics reveal the mechanism underlying the anti-atherosclerotic effects of aspirin eugenol ester on vascular endothelial dysfunction, Int. J. Mol. Sci. [Internet] 20 (13) (2019) 3165, https://doi.org/10.3390/ijms20133165.

[27] Y.-S. Kang, J.-C. Kim, J.-S. Kim, S.H. Kim, Effects of swimming exercise on serum irisin and bone FNDC5 in rat models of high-fat diet-induced osteoporosis, J. Sports Sci. Med. 18 (4) (2019) 596–603.

[28] H. Kuge, H. Mori, T. Morisawa, K. Hanyu, J. Miyazaki, M. Watanabe, et al., Effect of different dosages of ST36 indirect moxibustion on the skin temperature of the lower legs and feet, Medicines (Basel) [Internet] 5 (2) (2018), https://doi.org/10.3390/medicines5020057.

[29] L. Duan, G. Zhao, B. Ji, Y. Cao, X. Chen, Effect of crude-herb moxibustion on blood lipids in rats with dyslipidemia, J. Tradit. Chin. Med. Sci. [Internet] 1 (2) (2014) 140–147, https://doi.org/10.1016/j.jtcms.2014.11.011.

[30] X. Ye, H. Zhang, Influence of moxibustion temperatures on blood lipids, endothelin-1, and nitric oxide in hyperlipidemia patients, J. Tradit. Chin. Med. [Internet] 33 (5) (2013) 592–596, https://doi.org/10.1016/s0254-6272(14)60026-1.

[31] A. Rohatgi, M. Westerterp, A. von Eckardstein, A. Remaley, K.-A. Rye, HDL in the 21st century: a multifunctional roadmap for future HDL research, Circulation [Internet] 143 (23) (2021) 2293–2309, https://doi.org/10.1161/circulationaha.120.044221.

[32] H. Wang, L. Ha, X. Hui, Y. Lin, R. He, Z. Baixiao, Effect of moxibustion on hyperhomocysteinemia and oxidative stress induced by high-methionine diet, Evid. Based Complement Alternat. Med. [Internet] 2020 (2020) 1–8, https://doi.org/10.1155/2020/3184785.

[33] H.-F. Zhang, L.-L. Wang, M.-Y. Ji, X.-Y. Zhou, Effects of mild moxibustion on contents of blood lipoids and serum NO in hyperlipidemia rats, Zhongguo Zhen Jiu 33 (5) (2013) 438–442.

[34] J. Shen, T. Liu, X. Liu, J.-Y. Ge, H.-L. Wang, A.-L. Guo, et al., Effects of herbal-cake-separated moxibustion on the repair of vascular endothelial and SDF-1 in rabbits with atherosclerosis, Zhongguo Zhen Jiu [Internet] 39 (2) (2019) 173–178, https://doi.org/10.13703/j.0255-2930.2019.02.017.

[35] Y.-F. Zou, M.-Z. Ma, Z. Zhao, J. Tan, J.-J. Yang, J. Shi, et al., Effect of herbal-cake-separated moxibustion on blood lipid levels and expression of hepatic PPARγ and SR-B 1 proteins and genes in hyperlipidemia atherosclerosis rabbits, Zhen Ci Yan Jiu [Internet 43 (2) (2018) 86–91, https://doi.org/10.13702/j.1000-0607.170729.

[36] Q. Shao, J. Cheng, Y. Li, G. Ni, Liquid chromatography-mass spectrometry-based plasma metabolomics study of the effects of moxibustion with seed-sized moxa cone on hyperlipidemia, Evid. Based Complement Alternat. Med. [Internet] 2020 (2020), 1231357, https://doi.org/10.1155/2020/1231357.

[37] M. Ma, J. Jiang, X. Zhou, et al., Influence of suspended moxibustion on the biochemical markers of patients with hyperlipidemia, J. Acupunct. Tuina Sci. 6 (10) (2012) 364–367.

[38] D.L. Medina, D. Paola, S. Peluso, I. Armani, D. Stefani, D. Venditti, Lysosomal calcium signalling regulates autophagy through calcineurin and TFEB, Nat. Cell Biol. 17 (3) (2015) 288–299.

[39] Ahn JC, Lim JK. 肝俞) 및 중완혈 (中脘穴) 백서의 (白鼠) 혈청지질 변화에 미치는 영향. J. Korean Acupunct. Moxibust. Soc.. 11(1):283–295.

[40] L. Galluzzi, D.R. Green, Autophagy-independent functions of the autophagy machinery, Cell [Internet] 177 (7) (2019) 1682–1699, https://doi.org/10.1016/j.cell.2019.05.026.

[41] S. Tomczyk, N. Suknovic, Q. Schenkelaars, Y. Wenger, K. Ekundayo, W. Buzgariu, et al., Deficient autophagy in epithelial stem cells drives aging in the freshwater cnidarian Hydra, Development [Internet 147 (2) (2020), https://doi.org/10.1242/dev.177840 dev177840.

[42] V. Rogov, V. Dötsch, T. Johansen, V. Kirkin, Interactions between autophagy receptors and ubiquitin-like proteins form the molecular basis for selective autophagy, Mol. Cell [Internet] 53 (2) (2014) 167–178, https://doi.org/10.1016/j.molcel.2013.12.014.

[43] H. Obayashi, Y. Nagano, T. Takahashi, T. Seki, S. Tanaka, N. Sakai, et al., Histone deacetylase 10 knockout activates chaperone-mediated autophagy and accelerates the decomposition of its substrate, Biochem. Biophys. Res. Commun. [Internet] 523 (1) (2020) 246–252, https://doi.org/10.1016/j.bbrc.2019.12.048.

[44] R. Gómez-Sánchez, E. Pizarro-Estrella, S.M.S. Yakhine-Diop, M. Rodríguez-Arribas, J.M. Bravo-San Pedro, J.M. Fuentes, et al., Routine Western blot to check autophagic flux: cautions and recommendations, Anal. Biochem. [Internet 477 (2015) 13–20, https://doi.org/10.1016/j.ab.2015.02.020.

[45] D.G. Hardie, AMPK–sensing energy while talking to other signaling pathways, Cell Metab. [Internet] 20 (6) (2014) 939–952, https://doi.org/10.1016/j.cmet.2014.09.013.

[46] H.-Y. Yin, Y.-P. Fan, J. Liu, D.-T. Li, J. Guo, S.-G. Yu, Purinergic ATP triggers moxibustion-induced local anti-nociceptive effect on inflammatory pain model, Purinergic Signal [Internet] 19 (1) (2023) 5–12, https://doi.org/10.1007/s11302-021-09815-5.

[47] T.-Y. Liu, X.-Q. Xiong, X.-S. Ren, M.-X. Zhao, C.-X. Shi, J.-J. Wang, et al., FNDC5 alleviates hepatosteatosis by restoring AMPK/mTOR-mediated autophagy, fatty acid oxidation, and lipogenesis in mice, Diabetes [Internet] 65 (11) (2016) 3262–3275, https://doi.org/10.2337/db16-0356.

[48] R. Xia, W. Wang, B. Gao, Q. Ma, J. Wang, X. Dai, et al., Moxibustion alleviates chronic heart failure by regulating mitochondrial dynamics and inhibiting autophagy, Exp. Ther. Med. [Internet] 23 (5) (2022) 359, https://doi.org/10.3892/etm.2022.11286.

[49] H. Yueping, Y. Qin, O. Xiali, L. Yao, L. Yajie, H. Chang, et al., The mechanism study of moxa combustion products on regulating vascular endothelial function in atherosclerotic mice, Evid. Based Complement Alternat. Med. [Internet] 2022 (2022) 1–12, https://doi.org/10.1155/2022/1303978.

[50] Y. Jin-Liang, C. Jin, Effects of external thermal stimulation on the energy substance of human umbilical venous endothelial cells, China J. Tradit. Chin. Med. Pharm. 30 (1) (2015) 255–258.

[51] L. Xia, L. Mai-Lan, W. Hou-Lian, Regulatory effect of herbal cake-partitioned moxibustion on cholesterol reverse transport nuclear receptor LXRα in rabbits with atherosclerosis, J. Acupunct. Tuina Sci. (2019) 1–8.

[52] T. Zhu, Y. Ma, J. Wang, X. Chen, J. Li, L. Meng, et al., Grain-sized moxibustion heightens the AntiTumor effect of cyclophosphamide in Hepa1-6 bearing mice, Evid. Based Complement Alternat. Med. [Internet] 2022 (2022), 3684899, https://doi.org/10.1155/2022/3684899.

[53] B. Huang, Tissue Microdialysate Triggered by Moxibustion on Different Temperatures under Different States, 2019.

[54] Q. Ma, Whole-genome DNA Methylation Profile at Moxibustioned Site ST36, 2018.

[55] Y.-S. Wang, J.-B. Zhang, J.-F. Jiang, L.-L. Wang, Research on effects of the thermal stimulation by moxibustion at different temperatures on cardiac function in rats and on mast cells in the local site of moxibustion, Evid. Based Complement Alternat. Med. [Internet] 2013 (2013) 1–7, https://doi.org/10.1155/2013/545707.

[56] J.Y. Zong, The Influence of Different Temperature Moxibustion on Hyperlipidemia Mice Acupoint Area Skin and the Effect of Lipid Control Inflammation, 2018.

[57] H. Cai, Dose Effect of Dorsal Horn Responses at Different Moxibustion Temperatures Based on TRPV1, 2018.

[58] N. Zhang, N. Zhao, L.-S. Xie, B. Huang, S.-R. Lin, Q. Zhang, et al., Mitochondrial respiratory chain and its regulatory elements SIRT1 and SIRT3 play important role in the initial process of energy conversion after moxibustion at local skin, Evid. Based Complement Alternat. Med. [Internet] 2020 (2020) 1–10, https://doi.org/10.1155/2020/2343817.
[59] X. Cui, K. Liu, X. Gao, B. Zhu, Advancing the understanding of acupoint sensitization and plasticity through cutaneous C-nociceptors, Front. Neurosci. [Internet] (2022) 16, https://doi.org/10.3389/fnins.2022.822436.
[60] K. Huang, S. Liang, Z. Sun, J. Zhang, Startup mechanism of moxibustion warming and dredging function, Zhongguo Zhen Jiu [Internet] 37 (9) (2017) 1023–1026, https://doi.org/10.13703/j.0255-2930.2017.09.031.
[61] H. Kawanami, H. Kawahata, H.-M. Mori, M. Aoki, Moxibustion promotes formation of granulation in wound healing process through induction of transforming growth factor-β in rats, Chin. J. Integr. Med. [Internet] 26 (1) (2020) 26–32, https://doi.org/10.1007/s11655-019-3083-x.
[62] F. Hao, Q. Wang, L. Liu, L.-B. Wu, R.-L. Cai, J.-J. Sang, et al., Effect of moxibustion on autophagy and the inflammatory response of synovial cells in rheumatoid arthritis model rat, J. Tradit. Chin. Med. 42 (1) (2022) 73–82.
[63] C. Sun, Y. Li, J. Kuang, X. Liang, J. Wu, C. Ji, The thermal performance of biological tissue under moxibustion therapy, J. Therm. Biol. [Internet] 83 (2019) 103–111, https://doi.org/10.1016/j.jtherbio.2019.05.018.
[64] C.-Y. Jiang, C. Wang, N.-X. Xu, T. Fujita, Y. Murata, E. Kumamoto, 1,8- and 1,4-cineole enhance spontaneous excitatory transmission by activating different types of transient receptor potential channels in the rat spinal substantia gelatinosa, J. Neurochem. [Internet] 136 (4) (2016) 764–777, https://doi.org/10.1111/jnc.13433.
[65] W. Li, J. Liu, A. Chen, D. Dai, T. Zhao, Q. Liu, et al., Shared nociceptive dorsal root ganglion neurons participating in acupoint sensitization, Front. Mol. Neurosci. [Internet] (2022) 15, https://doi.org/10.3389/fnmol.2022.974007.
[66] N. Ding, J. Jiang, P. Qin, Q. Wang, J. Hu, Z. Li, Mast cells are important regulator of acupoint sensitization via the secretion of tryptase, 5-hydroxytryptamine, and histamine, PLoS One [Internet] 13 (3) (2018), e0194022, https://doi.org/10.1371/journal.pone.0194022.
[67] P. Verderio, M. Lecchi, C.M. Ciniselli, B. Shishmani, G. Apolone, G. Manenti, 3Rs principle and legislative decrees to achieve high standard of animal research, Animals (Basel) [Internet] 13 (2) (2023) 277, https://doi.org/10.3390/ani13020277.